A divergent protein kinase A in the human pathogen *Leishmania* is associated with developmental morphogenesis

Fischer Weinberger, R.[1], Bachmaier, S.[2], Dandugudumula, R.[1], Phan, I.Q.[3,4], Almoznino, M.[1], Githure, G.B. [2], Polatoglou, E.[2], Tsigankov, P.[1], Nitzan Koren, R[1]., Myler, P.J. [3,4,5], Boshart, M.[2] and Zilberstein, D.[1*]

[1]Faculty of Biology, Technion - Israel Institute of Technology, Haifa 32000, Haifa, Israel

[2]Faculty of Biology, Genetics, Ludwig-Maximilian University Munich, Großhaderner Straße 2-4, 82152 Martinsried, Germany

[3]Seattle Structural Genomics Center for Infectious Disease, Seattle, WA, USA

[4]Center for Global Infectious Disease Research, Seattle Children's Research Institute, 307 Westlake Ave N, Seattle, WA 98109-5219, USA.

[4]Department of Pediatrics, Department of Biomedical Informatics & Medical Education, and Department of Global Health, University of Washington, Seattle, WA 98195, USA

*corresponding author email: danz@technion.ac.il

Summary

Parasitic protozoa of the genus *Leishmania* cause human leishmaniasis. They cycle between the phagolysosome of mammalian macrophages, where they reside as round intracellular amastigotes, and the mid-gut of female sand flies, which are colonized by elongated extracellular promastigotes. Shifting promastigotes to a lysosome-like environment (pH 5.5 and 37˚C, 5% CO_2) initiates their development into amastigotes. Previous studies suggested a role for protein kinase A in this differentiation process. Here we describe a new, divergent, regulatory subunit of protein kinase A (PKAR3) present only in a limited group of kinetoplastids. In *L. donovani*, phosphorylation of PKAR3 is regulated by the differentiation signal and coincides with parasite morphogenesis during stage development. LdPKAR3 is bound to the subpellicular microtubules cell cortex *via* a formin FH2-like domain at the tip of a large and divergent N-terminal domain. Immunoprecipitation, fluorescence resonance energy transfer (FRET) and proteomics analyses show that PKAR3 selectively binds the C3 isoform of the PKA catalytic subunit in a holoenzyme complex, as supported by structural modeling. In promastigotes, PKAR3 recruits PKAC3 to the subpellicular microtubules at the cell's central cortex. After exposure to the differentiation signal, PKAR3 relocates evenly to the entire cortex in concert with cell rounding. Deleting either the R3 or C3 subunit resulted in premature rounding of the promastigote population, indicating that PKA determines their normal elongated shape. Regulation of *Leishmania* developmental morphogenesis by interaction with the subpellicular microtubule corset is a novel function for an unusual PKA complex not present in the host cell.

Keywords: differentiation, protein kinase A, signaling, microtubule cortex, morphogenesis, *Leishmania*, parasitism

Introduction

Leishmania donovani is a (trypanosomatid) protozoan parasite that causes kala azar, a fatal form of visceral leishmaniasis in humans [1]. These organisms cycle between the midgut of female sand flies, where they reside as flagellated extracellular promastigotes, and the phagolysosomes of mammalian macrophages, where they live as aflagellate amastigotes [3]. Infective metacyclic promastigotes are introduced into the host during the sand fly blood meal; after which they are phagocytosed by resident macrophages near the bite-site [5,6]. Once inside the host phagolysosome, promastigotes encounter two physical cues that distinguish this environment from that of the vector gut: acidic pH (~5.5) and elevated temperature (~37ºC). Promastigotes process these cues into a signal that initiates development into amastigotes [7,8,9]. However, the molecular details of this signaling pathway are still largely unknown.

Development of host-free systems using axenic parasites has advanced our understanding of the molecular mechanism of *Leishmania* intracellular development. *L. donovani* differentiation can be induced in culture, by exposing promastigotes to the high temperature and acidity (37°C, pH5.5, 5% CO_2) typically found in the phagolysosome [10,11,12]. Differentiation to mature amastigotes takes 5 days, similar to the time it takes *in vivo* [13]. Among the earliest events during *L. donovani* promastigote-to-amastigote differentiation are changes in the phosphorylation status of many proteins [14]. Significantly, while protein kinase A (PKA)-specific phosphorylation is common in promastigotes, most of these phosphoproteins are dephosphorylated within a few minutes after initiation of promastigote-to-amastigote differentiation [7]. This suggests that regulation of PKA activity is important for *Leishmania* development initiation.

PKA-mediated signaling pathways are ubiquitous in eukaryotic cells, implicated in growth control, development, and metabolism. The canonical PKA regulatory system in vertebrates involves assembly of two catalytic (PKAC) and two regulatory (PKAR) subunits into an inactive holoenzyme complex, mediated by dimerization and docking (D/D) domains in the N-terminal portion of PKAR [15]. When cAMP binds the cyclic nucleotide-binding domains (cNBDs) near the C-terminal of each PKAR, the resultant conformational change triggers dissociation of the PKAC-R complex and release of active PKAC subunits. Compartmentation to microdomains of PKA activity is achieved (at least in higher eukaryotes) through interaction of the D/D domain of PKAR with a diverse family of A-kinase anchoring proteins (AKAPs) that vary according to biological context [16]. However, PKARs from many lower eukaryotes (including trypanosomatids) appear to lack the D/D domain [17,18,19].

Most eukaryote genomes (with the notable exception of plants and algae) encode one or more PKAC subunits [18]. Trypanosomatids (including *L. donovani*) are no exception, usually having two subunits (C1 and C2) that are almost identical and a third (C3) that is more divergent [20]. Phosphoproteomic analyses of *L. donovani* revealed that all three PKAC subunits contain at least two phosphorylation sites [21]. One, within the kinase active site loop, matches the canonical PKA phosphorylation motif (RXXpS/pT) and is phosphorylated only in promastigotes. The second is located close to the C-terminus within a canonical ERK1/ERK2 substrate motif (pSP). LdPKAC1/C2 is phosphorylated at this site in promastigotes, but LdPKAC3 only after exposure to the differentiation signal [14]. In other eukaryotes, phosphorylation of both a threonine (T_{197}) in the activation loop and a serine (S_{338}) near the C-terminus is necessary for full activation

of PKAC, suggesting that C1 and C2 are active in *L. donovani* promastigotes, while C3 is apparently transiently activated only upon receiving the differentiation signal.

Most eukaryotes also possess one or more PKAR subunits, whose number and evolution are more dynamic than for PKAC [18]. All trypanosomatids have a regulatory subunit (PKAR1) that localizes to the flagellum of *Trypanosoma brucei* [22,23,24] and *L. donovani*, where it is expressed only in the promastigote stage [7,25]. However, in contrast to higher eukaryotes, trypanosomatid PKAR1 appears to be monomeric and unable to bind cAMP [17,19].

Interestingly, *L. donovani* (along with other *Leishmania* species and *Trypanosoma cruzi*, but not *T. brucei*) have a second regulatory subunit (PKAR3) [20], containing >10 sites that are dynamically phosphorylated and dephosphorylated during differentiation, implying that it has a role in differentiation [14]. However, until now, little information has been available concerning the potential role of PKAR3. Here, we show that LdPKAR3-LdPKAC3 holoenzyme complex is anchored to the subpellicular microtubule at the cell cortex *via* an FH2 formin domain. Upon exposure to the differentiation signal, the R3-C3 holoenzyme dissociates and R3 relocates along the subpellicular microtubules, while in parallel promastigotes round up to form amastigote-shaped cells. Association between LdPKAR3 and LdPKAC3 is necessary for maintenance of the elongated shape of *Leishmania* promastigotes since mutants that lack either LdPKAR3 or LdPKAC3 lose their normal shape. This study reports a morphogenetic phenotype in *Leishmania* development caused by a member of a novel and evolutionary divergent class of the PKA family of protein kinases, thereby shedding new light on the process initiating intracellular parasitism.

Results

Leishmania PKA regulatory subunits are evolutionary divergent.

Previous phylogenetic analyses of the PKAR subunits from a wide range of organisms revealed that they have undergone dynamic and divergent evolution during eukaryote history [18]. Analysis of the genomes available from 39 different species in the phylum *Euglenozoa* revealed that all taxa (except for *Perkinsela,* which is an obligate endosymbiont) contain 2-5 PKA catalytic subunits and one or two regulatory subunits (see **Table S2**). However, the latter are quite different from other eukaryotic PKARs in both sequence and domain structure (**Fig. 1**). Phylogenetic analysis revealed three distinct groups of PKAR sequences, with two of them being restricted to the *Euglenozoa* (**Fig. 1A**). Both the trypanosomatid sequences (PKAR1 and PKAR3) diverge widely from those found in other eukaryotes (including the RI and RII classes found in animals), even those of their closest relatives (*Trichomonas*, *Giardia* and *Naegleria*) in the Excavata supergroup. While both trypanosomatid PKAR1 and PKAR3 contain a conserved inhibitor/pseudo-inhibitor sequence motif (in the middle of the protein sequence) and two cyclic nucleotide-binding domains (cNBDs) in their C-terminal portion, they differ substantially from each other (and from PKARs in other organisms) in their N-terminal portion (**Fig. 1B**). Instead of the canonical dimerization and docking (D/D) domain found in many (but not all) other eukaryotes, all trypanosomatid PKAR1s contain an RNI-like domain, possibly explaining their inability to form a homodimer [17]. However, Leucine Rich Repeats (LRRs) in the RNI-like domain may mediate different protein-protein interactions. *Diplonema papillatum* and *Euglena gracilis* (both of which are free-living flagellates outside of the Kinetoplastea class), as well as *Bodo saltans* (a free-living

kinetoplastid) and *Paratrypanosoma confusum* (an early branching trypanosomatid parasite of mosquitoes) [26] all contain a second paralogue of this gene (PKAR2), with the *Euglena* version containing three additional pairs of cNBDs. Interestingly, Pcon_PKAR2 segregates outside the other Euglenozoan PKARs (and lacks the RNI-like domain), suggesting it may represent a more "ancestral" version. Many trypanosomatids contain second, more divergent, PKAR paralogue (PKAR3); but it is conspicuously absent from the Salivarian (*Trypanozoon* and *Nannomonas* sub-genera) *Trypanosoma* that lack an intracellular amastigote stage, as well as *Phytomonas* and *Herpetomonas*, which are the insect and/or plant pathogens in the Phytomonadinae subfamily. PKAR3 has a slightly longer C-terminal extension (following the cNBDs) and a much longer N-terminal region with no sequence similarity to other PKARs (**Fig. 1B**). This region contains no obvious protein domains or motifs, although HHpred analysis (https://omictools.com/hhpred-tool) identified weak structural similarity at the N-terminus of LdPKAR3 (but not those from other species) with a formin homology (FH2)-like domain.

Cytoskeletal localization of LdPKAR3 to cortical subpellicular microtubules.

Polyclonal antibodies raised in rabbits against recombinant LdPKAR3 reacted with a 72 kDa protein in wild-type cells (+/+ in **Fig. S1B**). This protein was absent in null mutants (-/- in **Fig. S1B**) but reappeared after ectopically expression of a full-length copy of the *LdPKAR3* gene in the null mutant (-/-/+ in **Fig. S1B**), thereby confirming its identity. Confocal microscopy using dual labeling with antibodies against LdPKAR3 and the plasma membrane of *L. donovani* promastigotes revealed that LdPKAR3 is localized to the cell cortex (**Fig. 2**). In promastigotes, LdPKAR3 is restricted to the cortex between the nucleus and flagella pocket; a region representing only 45% (±10%) of the cell length

(n=47 cells). In contrast, LdPKAR3 covers the entire cortex of both axenic and intracellular amastigotes (**Fig. 2**).

The *Leishmania* cell cortex contains an abundant rigid cytoskeleton made of stable subpellicular microtubules [27,28,29]. Previous studies have shown that non-ionic detergents can solubilize the trypanosomatid surface membrane and leave the subpellicular microtubules intact [30,31,32]. *Leishmania* cells treated with the zwitterion detergent n-dodecyl β-D-maltoside (DDM, 0.5%, which is neutral at pH 7) retained LdPKAR3 in the non-soluble pellet of promastigotes obtained both before, and 5 hours after, the differentiation signal (**Fig. 3A**). As expected, β-tubulin also enriched in the DDM-insoluble pellet (**Fig. 3A** and **Fig. S3A**). Indirect immunofluorescence using antibodies against β-tubulin indicated that this fraction contained the subpellicular microtubules, which retained the shape of promastigotes and amastigotes (**Fig. S3B**). Efficient solubilization of the parasite plasma membrane was confirmed by the absence of the integral membrane protein LdAAP24 [33] and the cytosolic HSP83 [11] in the enriched microtubules (**Fig. S3C**). Thus, we conclude that LdPKAR3 associates with the subpellicular microtubules cytoskeleton in *L. donovani* promastigotes.

Binding of PKARIβ to microtubules has been described previously in neuronal axons of mammalian cells [34], where binding is mediated by interaction between the dimerization and docking (D/D) domain of RIβ and a microtubule associated protein (MAP2) [35]. As indicated above (**Fig. 1B**), LdPKAR3 lacks the canonical D/D domain but instead contains an FH2-like domain at its N-terminus. FH2 is one of three cytoskeleton-binding domains found in formins, a diverse family of proteins that regulate cytoskeleton rearrangement in many eukaryotes [36], leading us to speculate that this domain might be

responsible for binding of LdPKAR3 to the subpellicular microtubules. To test this hypothesis, we ectopically expressed a truncated version of LdPKAR3 (lacking the N-terminal 90 amino acids that contains the FH2 domain) in mutant (*Δldpkar3*) promastigotes. As shown in **Fig. 3B**, add-back of full-length (*FL*) LdPKAR3 resulted in restoration of LdPKAR3 binding to the DDM-insoluble subpellicular microtubules; whereas the truncated version (Δ90) did not bind to the microtubules and remained in the supernatant. Hence, binding of LdPKAR3 to the microtubule cytoskeleton is mediated through the N-terminal FH2 domain. Interestingly, the truncated LdPKAR3 protein appears to undergo proteolytic cleavage in the supernatant (presumably by endogenous proteases released after cell lysis), suggesting that binding to the subpellicular microtubules is essential for its stability.

LdPKAR3 associates with a catalytic subunit to form a PKA holoenzyme.

To verify that LdPKAR3 can be categorized as regulatory subunit of PKA, we tested its interaction with the PKA catalytic subunits. Because no antibodies are available for the *L. donovani* PKAC isoforms, we expressed LdPKAR3-Ty1 under control of a tetracycline repressor in a *T. brucei Δpkar1* cell line [7,19]. The absence of TbPKAR1 in this cell line eliminates the possible competition with LdPKAR3 for interaction with TbPKAC subunits. As expected, expression of LdPKAR3-Ty1 increased in the presence of tetracycline (**Fig. 4A**), although some "leaky" background expression was present in the absence of tetracycline. Upon detergent fractionation of *T. brucei* **(Fig. 4B)** LdPKAR3 is found in the DDM-soluble supernatant as well as in the DDM-insoluble pellet, indicating that LdPKAR3 preserves the association with the cell cortex cytoskeleton as seen in *L. donovani* **(Fig. 3A)**. TbPKAC3 is enriched in the DDM-

insoluble fraction, suggesting that an R-C complex may be associated with the cell cortex cytoskeleton. Affinity purification of LdPKAR3-Ty1 from the DDM supernatant using anti-Ty1 antibody coupled to magnetic beads, and western blotting with antibodies against the TbPKAC subunits, indeed showed stable interaction of LdPKAR3-Ty1 with TbPKAC3 **(Fig. 4C),** but not with TbPKAC1/2 (**Fig. 4D**). Interestingly, up-regulation of LdPKAR3-Ty1 expression was accompanied by increased TbPKAC3 expression, possibly due to its stabilization in a complex with LdPKAR3 (**Fig. 4A**).

To further confirm the interaction between homologous LdPKAC3 and LdPKAR3, both proteins were co-expressed in *L. tarentolae* using the LEXSY expression system (Jena Bioscience) and the expected complex was purified by tandem affinity chromatography using the N-terminal His_6 tag on LdPKAR3 and Strep tag on LdPKAC3. The proteins were well expressed in the *L. tarentolae* cells and LdPKAC3 co-purified with LdPKAR3 (**Fig. 4E**). As positive control, the tagged LdPKAR1 and LdPKAC3 were co-expressed and co-purified in a parallel experiment (**Fig. 4F**) since a TbPKAR1/TbPKAC complexes were previously reported in *T. brucei* [19]. Thus, we conclude that the LdPKAR3 forms a stable a PKA catalytic subunit kinase, as expected for a regulatory subunit.

Western blot analysis of transgenic *L. donovani* WT and *Δldpkar3* promastigotes showed that HA-tagged LdPKAC3 was detected (at about the same level) in cell lysates of both the WT and mutant cell-lines (**Fig. 5A).** However, while LdPKAC3 was found in the DDM-enriched microtubule fraction of WT cells, it was present at only near-background levels in the microtubule fraction of *Δldpkar3*. These results were confirmed by proteomic analysis of the DDM-insoluble fraction of WT and *Δldpkar3* promastigotes

(Data are available via ProteomeXchange with identifier PXD025222). As expected, LdPKAR3 was readily detected in microtubules from WT cell, but not those from *Δldpkar3* (**Fig. 5B**); while LdPKAR1 was not detectable in any of the insoluble fractions. The relative abundance of LdPKAC3 (calculated from spectral counts for LinJ.18.1090) was ~30-fold higher in WT compared to *Δldpkar3* microtubules (**Fig. 5B**). Similar results were obtained with samples obtained from promastigotes before (0 hr), and 5 hours after, exposure to the differentiation signal, although LdPKAR3 and LdPKAC3 levels were usually somewhat lower at 5 hours. In contrast, other proteins, not involved with R3 association showed little difference in relative abundance between samples, as illustrated by the results for actin (ACT) shown in **Fig. 5B.** These experiments confirm that LdPKA-R3 is essential for recruitment of LdPKAC3 to the subpellicular microtubules.

We also employed the Fluorescence Resonance Energy Transfer (FRET) [37,38] to determine the molecular proximity of LdPKAR3 and LdPKAC3 within transgenic *L. donovani* promastigotes expressing HA-tagged LdPKAC3, as described in the STAR Methods. Control experiments using cells labelled separately with each of the secondary antibodies showed only background fluorescence, but no FRET (**Fig. S4**). However, FRET was clearly observed (as a high density of green dots) when both antibodies were added together (**Fig. 5C)**. Each dot represents a point of interaction between LdPKAR3 and LdPKAC3, with the color scale reflecting the intensity of interaction (*i.e.* proximity between the two molecules). These results further confirm the LdPKAR3-mediated recruitment of PKAC3 to form a (putative) holoenzyme localized to the subpellicular microtubules of the parasite cell cortex.

Structural analysis of the interaction between PKAR3 and PKAC3.

To-date, we have been unable to determine the structure of PKAR3 experimentally, although an X-ray structure is available for *T. cruzi* PKAR1 [19]. However, the mammalian PKAR and PKAC subunits have been extensively studied at the atomic level, both alone and in complex [39,40,41], allowing us to perform homology modeling based on these structures. The N-terminal sequence of LdPKAR3 protein is divergent from human (and other) PKAR subunits (see **Fig. 1B**) and is predicted to be mostly (except for the N-terminal 80 amino acids) low-complexity and disordered; this region was omitted, and models built using only the C-terminal portion of LdPKAR3, starting from the inhibitor/pseudo-inhibitor sequence. The equivalent region of *Bos taurus* (Bt) PKARIα (*i.e.* lacking a DD domain) forms a homodimer where the R/R interface acts as a cAMP sensor [40]. The residues responsible for the Bt R/R interaction are divergent in LdPKA-R3 (**Fig. 6A**), preventing the formation of critical hydrogen bonds between the $Y_{120}K_{121}$ side-chains of PKARIα ($Q_{350}E_{351}$ in LdPKAR3) and $R_{144}S_{145}$ ($I_{374}A_{375}$ in LdPKAR3) and suggesting that LdPKAR3 does not form a homodimer; thereby resembling the monomeric R subunit of trypanosomes [19]. In addition, the cAMP-binding sites of BtPKARIα are not conserved in LdPKAR3, with the strictly conserved residues in the mammalian cNBDs (R_{210} and R_{334} in BtPKARIα) that stabilize the cAMP phosphate replaced by N_{443} and A_{567} in LdPKAR3 (**Fig. 6B**). Furthermore, a change from R_{239}^{RI} to D_{473}^{R3} likely prevents the formation of a critical regulatory-salt bridge with an upstream residue ($E_{143}^{RI}/D_{373}^{R3}$) that strains the B/C helix between the cNBDs and favors the formation of the binding interface [42]. Similar non-conservative amino acid changes

are also found in LdPKAR1 (A_{319} and T_{443}), likely explaining why *T. equiperdum* and *T. brucei* PKAR1 bind neither cAMP nor cGMP [17,19].

Based on homology modeling to the mammalian PKARIα-C complexes, the salt-bridge triad (R_{240}^{R}-D_{266}^{R}-R_{194}^{C}) that stabilizes interaction between the regulatory and catalytic subunits appears to be conserved in *L. donovani* PKAR3 and PKAC3 (R_{475}^{R3}-E_{501}^{R3}-R_{166}^{C3}), as are the PKAC activation loop (T_{169}^{C3}) and the regulatory salt-bridge (Q_{495}^{R3}-R_{601}^{R3}) responsible for PKA activation (**Fig. 6C**). However, other residues involved in regulation of PKA catalytic activity by BtPKARIα are not conserved. For example, non-conservative replacement (R_{95}^{RI}/S_{324}^{R3}) of the first residue in the predicted LdPKAR3 inhibitor/pseudo-inhibitor site is predicted to disrupt interaction with negatively charged and polar residues (T_{23}, E_{99}, E_{142} and Y_{302}) in LdPKAC3 (**Fig. 6D**).

Polar localization of LdPKA-R3 is developmentally regulated and associated with morphogenesis.

To better characterize the changes in LdPKAR3 localization along the cortex subpellicular microtubules during development from promastigotes to amastigotes, we used immunofluorescence to examine DDM-insoluble fractions obtained at various times following exposure to the differentiation signal (**Fig. 7)**. Control experiments (**Fig. S3D**) indicated that subpellicular microtubules from the Δ*ldpkar3* mutants showed no background fluorescence with antibody against LdPKAR3. Counter-staining with antibodies against β-tubulin shows that LdPKAR3 localizes largely to the central region of the cytoskeleton in promastigotes before differentiation (**Fig. 7**, left column), confirming the localization seen in intact cells (**Fig. 2**). In contrast, the subpellicular microtubules of fully differentiated axenic amastigotes (120 hours) were uniformly

labeled by LdPKAR3 (**Fig. 7**, right column). Indeed, LdPKAR3 was already uniformly distributed over the entire subpellicular microtubule network as early as 12 hours after exposure to the differentiation signal (**Fig. 7**, middle column). Thus, it appears that LdPKAR3 mobilization correlates with the timing of parasite rounding, which begins ~7 hours and is largely complete by 12 hours, as we have previously described during phase II of differentiation [9].

These "coordinated" events prompt us to hypothesize that an intact LdPKAR3-C3 holoenzyme at the central region of the subpellicular microtubules is necessary for maintaining the elongated shape of promastigotes. To assess this hypothesis, we investigated whether deleting the genes that encode either LdPKAR3 or C3 cause promastigotes to lose their elongated shape. Promastigotes of wild type and mutants lacking R3 (Δ*ldpkar3*) or C3 (Δ*ldpkac3)* were subjected to Image Streaming [434445] and confocal fluorescence analysis. The Image Streaming software was used to calculate the aspect ratio of individual cells and segragate them into three groups; elongated (**Fig. S5** panel A top and panel B top left), round (**Fig. S5** panel A bottom and panel B bottom**),** and intermediate shape we named "ovoid" (**Fig. S5** panel A top & bottom and panel B top right). These shapes were used as templates to analyze 10,000 cells of each group for each sample. The majority (53%) of WT promastigotes were elongated, with only 16% round (**Fig. 8A)**. In contrast, the proportion of round cells increased to 44% in the *Δldpkar3* mutants, while 49% of *Δldpkac3* mutants were rounded. The proportion of elongated cells in these mutant populations decreased to 20% and 18%, respectively; while the proportion of "ovoid" cells (36% and 33%, respectively) remained similar to that in WT (31%). Ectopic expression of the full-length *LdPKAR3* or *LdPKAC3* genes in

the null mutants partially restored the ratio of elongated to rounded cells (38%:26% and 31%:30%) to WT levels (53%:16%). Confocal fluorescence analysis using the anti-membrane antibodies confirm the shape changes enforced by both C3 and R3 gene deletion (**Fig. 8B**).

The results in **Fig. 8** indicate that it is the interaction between LdPKAR3 and LdPKAC3 and localization of the holoenzyme to the central region of the subpellicular microtubules that is important for maintenance of an elongated cell morphology in *Leishmania* promastigotes.

Discussion

Upon entry into their mammalian host, *Leishmania* promastigotes are ingested into macrophage phagolysosomes, where lysosome-specific environmental signals, such as acidic pH (~5.5) and body temperature (~37°C) act as cues for differentiation into amastigotes [11,46,47,48]. Our previous studies identified protein kinase A (PKA) as a potential key enzyme in this process [7]. Now, we have identified and characterized a highly divergent regulatory subunit of *Leishmania* PKA (LdPKAR3) as another key player in promastigote-to-amastigote differentiation. In promastigotes, LdPKAR3 is localized to subpellicular microtubules in the central region of the cell cortex, where it associates with the catalytic subunit isoform PKAC3. This kinase localization is essential for maintenance of the elongated morphology typical of promastigotes since loss of either subunit results in cellular rounding (and shortening of the flagellum). Upon exposure to the differentiation signal, LdPKAR3 relocates from its original location to the entire cell cortex, coinciding with the time into differentiation when promastigotes assume the rounded morphology of amastigotes.

To date, studies on the role of the microtubule cytoskeleton on *Leishmania* development and morphogenesis have focused mostly on the flagella [49,50]. The complex axoneme structure and its dynamics during differentiation from the flagellated promastigotes to the aflagellated amastigotes attracted significant attention. Promastigotes axoneme has the typical 9+2 structure. During differentiation into amastigotes the flagella shorten and then collapse to become a sensory flagellum with a 9+0 arrangement inside the flagella pocket [51]. Because flagella shortening paralleled change in cell morphology, it was believed that these processes are linked. However, using mutant promastigotes whose flagella shortened and transformed to the sensory 9+0 proved the opposite; flagella shortening and morphogenesis are not linked processes [52]. To

our knowledge the process of morphological change during parasite differentiation has not been further investigated. In this study we identified that a divergent PKA, of which the regulatory subunit exists only in the genome of a limited group of kinetoplastids, is essential for the elongated shape of promastigotes. The differentiation signal activates the relocation of LdPKAR3 along the entire subpellicular microtubule cortex, in parallel to rounding to amastigote-shaped cells. The observation that a novel regulatory subunit of PKA plays a role in *Leishmania* morphogenesis supports the notion that this process is not evolutionary conserved among the parasite and its hosts. In higher organisms it is mainly actin together with myosin motor proteins that is responsible for cell morphogenesis [53,54]. These observations open the door for more in-depth studies into the role of microtubules in remodeling cell shape and differentiation-induced morphogenesis.

We used four independent methodologies to demonstrate that LdPKAR3 forms a holoenzyme complex with LdPKAC3. Firstly, co-immunoprecipitation of LdPKAR3 and PKAC3 ectopically expressed in *T. brucei* and *L. tarentolae* showed their tight and stable interaction. Secondly, proteomic analysis of the DDM-enriched subpellicular microtubules showed that LdPKAR3 associates with LdPKAC3 in *L. donovani*. Thirdly, confocal immunofluorescence combined with FRET analysis confirmed the proximity of LdPKAR3 and LdPKAC3 at the parasite cell cortex of *L. donovani*. Finally, molecular modelling showed that some essential amino acid residues at the interaction interface between the mammalian PKA catalytic and regulatory subunits are conserved in LdPKAR3 and LdPKAC3. However, LdPKAR3 is missing a salt bridge contributing to PKAR dimerization of higher eukaryotes, as well as lacking the D/D domain and canonical cAMP binding sites. Thus, we conclude that *Leishmania* PKAR3 forms a R-C heterodimer and that its activation is independent of cAMP as

shown for the *T. brucei* orthologue [17,19]. It is currently not known whether LdPKAC3 is able to bind an alternative (unknown) ligand similar to TbPKAR1 [19].

In higher eukaryotes, PKARIβ is anchored to the abundant microtubule of axons by interacting the dimerization/docking domain (D/D) with the microtubule associated protein 2 (MAP2) [55]. The N-terminal portion of LdPKAR3 is largely unstructured and lacks a canonical D/D; so, the LdPKAC3-R3 holoenzyme is likely a heterodimer, similar to PKAC1-R1 in *T. brucei* [19,20]. Trypanosomatids lack MAP2 orthologues, which appear later in vertebrate evolution [55]. The presence of a predicted FH2 domain at the N-terminus of LdPKAR3 and the importance of this domain for localization raise the intriguing possibility that it mediates binding to subpellicular microtubules within the cell cortex of *Leishmania,* thus suggesting evolution of an alternative PKA tethering mechanism distinct from the mammalian D/D domain to MAP2 interaction. In other organisms, FH2 is one of three domains found in formins, a family of proteins involved in cell shape determination, adhesion, cytokinesis, and morphogenesis by remodeling actin or microtubule cytoskeletons [56,57]. However, the absence of significant HHpred matches for this region in other PKAR3 orthologues (including most *Leishmania* species) challenges this hypothesis.

PKAR1 retains conserved amino acid interactions at inhibitor/pseudo-inhibitor site and functions as a ligand dependent PKAC inhibitor, as reported previously for *T. brucei* PKAR1 (Bachmaier et al., 2019). A non-conservative change in the LdPKAR3 inhibitor/pseudo-inhibitor site may weaken the ability of LdPKAR3 to act as a pseudo-substrate and inhibitor for the catalytic subunit. Conversely, both S_{329}^{R3} and S_{332}^{R3} are predicted to be equally distant in space from T_{169}^{C3}, thereby allowing phosphorylation of either to cause the same repulsion effect that phosphorylation of S_{101}^{R} (which corresponds to S_{329}^{R3}) exerts on T_{197}^{C} of the bovine PKA-R/C

complex. This phosphorylation is postulated to enhance catalytic activity even without cAMP stimulation [58]. Therefore, it remains possible that LdPKAR3 regulates PKA catalytic activity by a mechanism independent of ligand binding. Interestingly, phosphorylation at S_{332} is up-regulated two-fold immediately after exposure to the differentiation signal [14], which may explain the increase in PKA-mediated phosphorylation at LdPKAR3 T_{262} early in differentiation.

In summary, this study is the first to characterize a new, divergent PKA regulatory subunit (LdPKAR3) that appears to be restricted to trypanosomatids with an intracellular lifecycle stage. The observation that LdPKAR3 is bound to the subpellicular microtubule and migrates upon exposure to the differentiation signal suggests that it may be part of the lysosome sensing pathway involved in initiating parasite differentiation inside its host [48]. We are currently investigating the mechanism by which LdPKAR3 and LdPKAC3 influence differentiation-related morphogenesis.

Acknowledgements

We thank the Smoler Proteomics Center at the Technion for all proteomic analyses. Funding for this work was provided by the USA-Israel Binational Foundation, grant number 2017030 to DZ and PJM; the German-Israel Foundation grant number I-112-416.10-2017 to DZ and MB; and contract HHSN272201700059C from the National Institute of Allergy and Infectious Diseases to PJM.

Author contributions

RFW, SB, RB, MA, PT and RNK conducted the experiment. IQP conducted the structure modeling analysis. GBG and EP conducted the bioinformatics and phylogenetics analyses. PJM supervised all bioinformatics and phylogenetic analysis and contributed to writing the manuscript. MB supervised the analyses in the heterologous systems. DZ managed the project and wrote the manuscript.

Declaration of interests

The authors declare no competing interests.

Figure legends

Fig. 1: Phylogenetic analysis of PKA regulatory subunits. A) Maximum-likelihood phylogenetic trees were constructed using the RaxML module of Geneious on a MAFFT alignment of amino acid sequences of the PKAR orthologues from 39 Euglenozoan species and 14 other species in the Amoebozoa, Apusozoa, Archaeplastida, Excavata, Opisthokonta or SAR (Stramenopiles/Alveolata/Rhizaria) supergroups. Red dots indicate PKAR orthologues containing a canonical (red fill) or non-canonical (light red fill) dimerization/docking (D/D) domain. Green dots indicate PKAR orthologues containing an RNI-like domain, which may mediate interaction with other proteins. **B**) Schematic representation of the protein domains within selected PKAR orthologues. The cAMP binding domains are indicated by blue boxes, the dimerization domain in red (canonical) or light red (non-canonical) and the RNI-like domain in green; with the inhibitory (pseudo-)phosphorylation sites marked by a brown or tan box.

Figure 2: LdPKAR3 relocates from the central region of the cortex in promastigotes to the entire cell cortex during differentiation to axenic and intracellular amastigotes. Indirect immunofluorescence of LdPKAR3 in promastigotes (left column), axenic (middle column) and intracellular amastigotes (48 hours post THP1 macrophage infection, right column). Cells were stained with antibodies against LdPKAR3 (upper row, green) and anti-membrane (middle row, red). Fluorescence was detected using a Zeiss LSM 700 inverted confocal microscope. Scale bar = 5 μm.

Figure 3: LdPKAR3 is bound to the subpellicular microtubules of *L. donovani via* a FH2 formin domain. A) The subpellicular microtubules were extracted from wild type *L. donovani* promastigotes before and five hours after exposure to the differentiation signal, using 0.5% DDM (details in STAR Methods). Proteins from whole cell lysates, DDM-insoluble pellet (P) and soluble supernatant (S) were separated on 10% SDS-PAGE and then subjected to western blot, using anti-LdPKAR3 (upper row), anti-HSP83 (a soluble protein marker, middle row) and anti-β tubulin (microtubule-rich fraction, lower row). **B**) A peptide of 90 amino acids from the LdPKAR3 protein was truncated (Δ90 LdPKAR3) as described in STAR Methods. Plasmids expressing this construct and the full-length add back were expressed in Δ*ldpkar3*. These and wild type promastigotes were subjected to subpellicular microtubules enrichment (0.5% DDM) and then subjected to western blot using anti-LdPKAR3 (upper row) and anti-β tubulin (lower row). (*) **C** indicates whole cell lysates, **P** indicate DDM-insoluble pellet and **S** indicates DDM soluble supernatant.

Fig. 4: LdPKAR3 interacts with the PKAC3 subunits. (A-D) LdPKAR3 with a C-terminal Ty1-tag was tetracycline-inducibly (+/- Tet) expressed in *T. brucei* MiTat 1.2 *pkar1* null cells (Δ*tbpkar1* LdPKAR3-Ty1) [7]. (A) Western blot with anti-PFR-A/C as loading control; LdPKAR3-Ty1 and TbPKAC3 are detected with expected molecular mass using anti-LdPKAR3 and anti-TbPKAC3 antibodies, respectively. (B) DDM extraction using the microtubule-associated protein TbSAXO [30] as marker for detergent resistance. Whole cell lysate (WCL), soluble fractions 1 and 2 (sol) and detergent-

resistant pellet (P) show detergent resistance of a fraction of LdPKAR3-Ty1 and enrichment of TbPKAC3 in the pellet fraction. (C-D) The DDM-soluble fractions of LdPKAR3-Ty1 and of the parental Δ*tbpkar1* cell line were subjected to anti-Ty1 pull down followed by detection of LdPKAR3-Ty1, TbPKAC3 (C) and TbPKAC1/2 (D) on western blots with rabbit anti-LdPKAR3, anti-TbPKAC3 (C) and anti-TbPKAC1/2 (D). IN = input; FT = flow-through; E = elution; M = molecular weight marker. (E-F) Purification of PKA holoenzyme complexes. (E) His_6-LdPKAR3 and Strep-LdPKAC3 or (F) His_6-LdPKAR1 and Strep-LdPKAC3 were co-expressed in *L. tarentolae* and tandem affinity purified. The soluble input (IN) and eluates (E1, E2) were analyzed by western blot and probed with mouse monoclonal anti-His (Bio-Rad), anti-Strep (Qiagen) and rabbit anti-LdPKAR3 or anti-TbPKAR1 (cross-reacting with LdPKAR1 [7].

Figure 5: LdPKAC3 binding to the subpellicular promastigotes is mediated by LdPKAR3. A) *L. donovani* promastigote WT and Δ*ldpka-r3* (ΔR3) cell lines expressing HA-tagged LdPKAC3 (C3) were subjected to subpellicular microtubule enrichment (0.5% DDM). Proteins from these fractions were subjected to western blot using anti-HA (upper row), antiLdPKA-R3 (middle row) and anti-β-tubulin (lower row). **B**) Proteins from DDM-enriched subpellicular microtubules from WT and Δ*ldpkar3* were loaded on a 10% SDS PAGE. A slice containing proteins at the molecular mass range of 35-42 kDa was excised and subjected to mass-spectroscopy (Orbitrap, Thermo, Ltd). The area below the graph of LdPKAC3 (LinJ.18.1090), LdPKAR3 (LinJ.34.2680) and LdACT (actin, LinJ.04.1250). Their abundance relative to the abundance in WT (set to 7000) is illustrated in promastigotes before (■, ■) and five hours after exposure to the

differentiation signal (■, ■). **C)** Fluorescence Resonance Energy Transfer (FRET) of LdPKAR3-C3 association at the cell cortex. Promastigotes of *L. donovani* WT and of a cell line ectopically expressing HA-tagged LdPKAC3 were labeled with rabbit anti-LdPKAR3 (endogenous protein) and mouse anti-HA. Subsequently, cells were labeled with secondary antibodies, anti-rabbit conjugated to Alexa fluor 568 and anti-mouse conjugated to Alexa fluor 647. The emission spectrum of Alexa flour 568 overlaps with the excitation spectrum of Alexa 647. The FRET emission color and strength were calculated using Axio Vision program (details in Materials and Methods). The color scale ruler on the left of each panel indicates the strength of FRET emission.

Figure 6: 3D modeling of LdPKAR3-C3 interaction. Homology models of LdPKA-R3 were built based on mammalian structures of PKARIα and PKACα from *Bos taurus*. **A**) Protein sequence alignment of LdPKA-R orthologues with *Bos taurus* (bovine) PKARIα (Bt_R_2qcs). **B**) 3D modelling of the predicted LdPKAR3 cyclic nucleotide binding domains based on bovine PKARIα. **C**) LdPKAR3-C3 interacting amino acids are conserved. Side-chains of residues involved in the regulatory salt-bridges and potential electrostatic interactions downstream of the pseudo-substrate are shown on the ribbon diagram of LdPKAR3 (magenta) and LdPKA-C3 (blue). **D**) Side chains of critical residues involved in the PKAR-PKAC interaction for *Bos taurus* BtPKARIα-PKACα (left) and *L. donovani* LdPKAR3-PKAC3 (right) are depicted. Note the R95S substitution in the LdPKAR3 pseudo-inhibitor residue compared to BtPKARIα.

Figure 7: LdPKA-R3 relocates on the subpellicular microtubules during promastigote to amastigote differentiation. Promastigotes before, 12 hours after exposure to the differentiation signal and mature amastigotes were subjected to 0.5% DDM enrichment of subpellicular microtubules. These were subjected to dual fluorescence staining using anti-LdPKAR3 (green, upper row) and anti-β-tubulin antibodies (red, middle panel). Merging the two fluorescent channels indicates the localization of R3 on the microtubules (lower row).

Figure 8: Deleting the genes encoding R3 or C3 turn promastigotes into round shaped cells. Mid log culture of *L. donovani* promastigotes of WT, Δ*ldpkar3*, Δ*ldpkar3* and their respective addbacks were subjected to image streaming (Amnis® ImageStream®X Mk II). **A**) the graph illustrates percentage of round (■) and elongated (■) cells. The number of ovoid cells was around 30% in all cell lines and therefore was not included in the graphs. **B**) bright field (upper row) and anti-membrane immunofluorescence of the cell lines from (A). The asterisks (* and/**) in (A) indicate statistical significance of $p < 0.05$ (significantly different from WT) and $p < 0.01$ (significantly different from WT), respectively, $n = 3$. The bars in (B) indicate 5 µm.

STAR Methods

Phylogenetic analysis of PKA regulatory subunits. The amino acid sequences of the PKAR orthologues from 39 species of Euglenozoa and 14 other eukaryotic species, including at least one in each of the Amoebozoa, Apusozoa, Archaeplastida, Excavata, Opisthokonta and SAR (Stramenopiles/Alveolata/Rhizaria) supergroups, were downloaded from the TriTrypDB, GenBank or Euglena International Network (EIN) databases (see Supplementary Table S2). The sequences were aligned using the MAFFT module of Geneious Prime 2021.1.1 (https://www.geneious.com) and a phylogenetic tree constricted using the RAxML (Randomized Axelerated Maximum Likelihood) version 8.2.11 [59] module implemented in rapid hill-climbing mode with joint branch length optimization and the BLOSUM62 Substitution Matrix. A GAMMA model of rate heterogeneity was used for ML estimate of alpha-parameter from 100 distinct randomized MP trees. Protein domains were identified using the InterProScan module of Geneious [60] and/or the HHpred website of the MPI Bioinformatics Toolkit [61,62].

Cells and culture. *L. donovani* MHOM/SD/00/1S [11] axenic promastigotes were grown in Earle's-based medium 199 (M199; Biological Industries, Ltd) supplemented with 10% heat-inactivated Fetal Bovine Serum (GIBCO, Ltd) and 1% Penicillin-Streptomycin solution (Biological Industries, Ltd). Axenic differentiation of *L. donovani* promastigotes to amastigotes was carried out as described previously [12]. Briefly, mid log phase promastigotes washed twice in EARL's salt solution and finally suspended in amastigote medium containing M199 at pH 5.5 supplemented with 0.5 mM sodium succinate, 25% fetal calf serum and 1% Penicillin-Streptomycin solution (differentiation

medium). Mature amastigotes developed at five days after exposing promastigotes to the differentiation medium. Trypanosomes were cultivated at 37°C and 5% CO_2 in modified HMI-9 culture medium [63] supplemented with 10% heat-inactivated fetal bovine serum. Cell density was kept below 1×10^6 cells/ml by regular dilution.

Cloning. PCR products and the plasmid vectors (see **Table S1**) were digested by restriction enzymes for 30 minutes at 37°C (FastDigest enzymes, Thermo Scientific) and ligated (T4 DNA ligase, Thermo Scientific) for up to 1 hour at 22°C. Ligation products were transformed into *E. coli* DH5α strain using heat-shock (42°C), incubated for 1 hour in Luria Broth (LB) medium at 37°C and plated on LB-agar plates supplemented with ampicillin. LB-agar plates were incubated at 37°C overnight. Bacteria colonies were screened using PCR or colony cracking method. Positive colonies were grown overnight in LB medium supplemented with ampicillin, and plasmids were extracted using a mini-prep kit (GeneJet Plasmid Miniprep Kit, Thermo Scientific). Extracted plasmids were sequenced to assure that no mutations were inserted during PCR or the cloning procedure.

Generation of a polyclonal anti-PKAR3 antibody. The full-length CDS of LdPKAR3 (encoded by *LinJ.34.2680*[1]) was PCR amplified from genomic DNA of *L. infantum* strain JPCM5 using primers (**Table S1**) designed to introduce an N-terminal His_6 tag followed by a TEV protease cleavage site and cloned *via Bam*HI and *Not*I restriction sites into pETDuet-1 (Novagen, Merck Millipore). The protein was expressed in *E. coli* Rosetta and purified using Ni-NTA columns followed by TEV protease

[1] To maintain consistency with our previous publications, we use the original GeneIDs for the *L. infantum* JPCM5 reference genome in TryTrypDB, rather than those for any of the *L. donovani* genomes.

cleavage. Recombinant LdPKAR3 was injected to two rabbits with 5 mg/ml protein each. Rabbits were boosted four times with 5 mg/ml of the recombinant LdPKAR3. Injections and bleedings were carried out as a contracted service (Sigma-Aldrich, Ltd).

Western blotting. Western blot analysis was done as described previously [64], using a 1:1,000 dilution of polyclonal rabbit anti LdPKAR3, TbPKAR1 [7], TbPKAC1/C2 [19] and TbSAXO [30]. Rabbit antibodies against TbPKAC3 was used at 1:250 dilution [19]. For Western blot detection of proteins recombinantly expressed in *L. tarentolae*, additionally the primary antibodies mouse anti-His (Bio-Rad) and mouse anti-Strep (Qiagen) were used. The secondary antibodies IRDye680LT goat anti-rabbit (1:50000; LICOR) and IRDye800CW goat anti-mouse (1:10000; LICOR) were used for detection with the Odyssey™ CLx imaging system (LICOR). Rabbit antiserum against *L. donovani* HSP83 [11] or β-tubulin (cell signalling #2146) were used as protein loading marker.

Gene knockouts. The gene encoding LdPKAR3 was deleted from the 1S-2D clone of *L. donovani* using homologous recombination as described previously by Inbar et al. [33]. PCR analyses of genomic DNA was used to confirm the absence of the targeted gene (**Figure S1A**). Polyclonal antibodies raised in rabbits against recombinant LdPKAR3 reacted with a protein of the correct molecular mass (72 kDa) in Western blots of wild type cells, but not *Δldpkar3* mutants (+/+ and -/-, respectively in **Figure S1B**). The protein was present (at slightly elevated levels) in add-back mutants (-/-/+) ectopically expressing full-length LdPKAR3.

LinJ.18.1090 (which encodes LdPKAC3) was deleted from the 1S-2D clone of *L. donovani* using the same strategy as LdPKAR3 above [33]. PCR analyses of *L. donovani* genomic DNA extracted from single colonies confirmed that both copies of the gene are

missing from *Δldpkac3*, while the antibiotic resistance genes that were inserted to replace LdPKAC3 are in place (**Fig. S1**).

Inducible overexpression of LdPKAR3 in Trypanosoma brucei. The *LdPKAR3* CDS was PCR amplified from genomic DNA of *L. donovani* promastigotes using primers LdPKAR3_HindIII_fw and LdPKAR3_lr_Ty1_BamHI_rev (**Table S1**) to introduce a C-terminal Ty1 tag. The PCR product was cloned into the *Hin*dIII and *Bam*HI sites of pHD615 [65], which was then linearized with *Not*I for transfection of a previously described homozygous *T. brucei* PKAR deletion mutant [7] that additionally expresses a double tetracycline repressor (pHD1313; [66]. Transfected cells were selected with 2 µg/ml blasticidin (pHD615) and 2.5 µg/ml phleomycin (pHD1313). *LdPKAR3* expression was induced with 1 µg/ml tetracycline.

Immunofluorescence. Indirect immunofluorescence analysis was carried out following the methods described by Inbar et al. [33]. Briefly, mid-log phase promastigotes were washed twice in phosphate buffered saline (PBS) and then fixed in 1% formaldehyde/PBS on a slide for 10 min before permeabilization by exposure to 0.2% TritonX-100/PBS for 10 min. Cells were incubated with blocking solution [5% (v/v) non-fat dried skimmed milk powder/PBST] for 30 min at room temperature, incubated with rabbit anti-LdPKAR3 (this study), rabbit anti-promastigote membrane proteins [11] or mice anti-HA tag antibodies (1:500 dilution) for one h. Subsequently, slides were washed three times with PBS-Tween and incubated with the fluorescent secondary antibody in darkness for 30 min. Slides were washed three time with PBS-Tween and a drop of DAPI Fluoromount G (Southern Biotech Ltd) was added. Slides were covered with slips, sealed, and then kept in darkness. Subsequently, they were examined using a Zeiss LSM

700 inverted confocal laser scanning microscope. Image processing was done using Zen lite software, Zeiss.

Image streaming. Image Streaming analysis was carried out using Amnis® ImageStream®X Mk II)[43,44,45]. The Image Streamer was calibrated by feeding it with late log phase axenic promastigotes and amastigotes. For each cell, a snapshot was taken, and the aspect ratio was calculated. The streamer divided these populations into three groups; elongated (**Fig. S4A top, B top left**), round (**Fig. S4A bottom, B bottom),** and intermediate shape we named ovoid (**Fig. S4A top and bottom, B top right**). Note that round promatigotes are flagellated whereas round amastigotes are aflagellated. These shapes were used as templates to analyze 10000 cells of each experimental group.

Detergent enrichment of subpellicular microtubules. Axenic *L. donovani* promastigote and parasites at various time points after exposure to the differentiation signal (20 ml of cells at 1×10^7 cells/ml) washed twice with ice-cold phosphate buffered saline (PBS). The final pellet suspended to 200 µl PBS containing protease inhibitors mix (Roche cOmplete protease inhibitor) and 0.5% n-dodecyl β-D-maltoside (DDM) in Eppendorf tubes. After a short vortex, the tubes were placed on ice for 15 min, and subsequently centrifuged (14,000 RPM for 15 min at 4°C). The pellet washed twice with 1 ml of ice-cold PBS containing the protease inhibitors. For immunofluorescence analysis, the pellet was suspended in 100 µl PBS. For Western blot analysis, the pellet was suspended in 100 µl Laemmli buffer. *T. brucei* subpellicular microtubules were enriched employing the same protocol used for *Leishmania*.

Immunoprecipitation in T. brucei. Immunoprecipitation of LdPKAR3-Ty1 was performed by binding anti-Ty1 [67] to magnetic protein A beads (Dynabeads, Invitrogen)

followed by a 2-hour incubation with 1×10^8 trypanosomes lysed in lysis buffer (10 mM Tris/Cl pH 7.5; 150 mM NaCl; 0.5 mM EDTA; 0.5% NP-40; Roche cOmplete protease inhibitor) for 30 min at 4°C. Beads were washed 4x with lysis buffer and proteins were eluted by incubation with 50 µl 2x Laemmli sample buffer for 5 min at 95°C.

Tandem affinity purification from Leishmania tarentolae. LdPKAR1 and LdPKAR3 were N-terminally tagged with a hexa-histidine peptide by PCR amplification from *L. donovani* genomic DNA. The PCR products were inserted in the pLEXSY_I-ble3® vector (Jena Bioscience). LdPKAC3 was N-terminally strep-tagged and inserted into pLEXSY_I-neo3®. The vectors were then linearized with *Swa*I and stably co-transfected for holoenzyme expression (LdPKAR1 and LdPKAC3 or LdPKAR3 and LdPKAC3) into the LEXSY T7-TR® cell line (Jena Bioscience). Protein co-expression, parasite cultivation and protein purification were performed as described in Bachmaier et al. [19] with a few modifications. Briefly, co-expression was induced with 10 µg/ml tetracycline for 48 hours. The cells were harvested by centrifugation (2000g for 5 min), washed with PBS, and lysed in His binding buffer (50 mM NaH_2PO_4 pH 8, 300 mM NaCl, 10 mM imidazole, 1% Triton-X, protease inhibitor cocktail). The soluble fraction was loaded on to a gravity flow Ni-NTA column (Thermo Fisher Scientific). The column was washed twice with His wash buffer (50 mM NaH_2PO_4 pH 8, 300 mM NaCl, 20 mM imidazole) before elution of the kinase complex was with His elution buffer (50 mM NaH_2PO_4 pH 8, 300 mM NaCl, 250 mM imidazole). The Ni-NTA eluate was loaded on to a gravity flow Strep-Tactin column (IBA), which was then washed with Strep wash buffer (50 mM NaH_2PO_4 pH 8, 300 mM NaCl). Lastly, the kinase complexes were eluted

with Strep elution buffer (50 mM NaH_2PO_4 pH 8, 150 mM NaCl, 50 mM biotin). The integrity of the co-expressed holoenzyme complexes was analysed by western blot.

Fluorescence Resonance Energy Transfer (FRET). Mid-logarithmic phase *L. donovani* promastigotes ectopically expressing LdPKAC3-HA were fixed in PBS containing 4% paraformaldehyde and then settled on slides. LdPKAR3 was labelled using polyclonal anti-R3 antibody (1:500), followed by detection with goat anti-rabbit Alexa 568 (1:500). LdPKAC3 was labelled with anti-HA antibody (1:1000, BioLegend#MMS-101P) and secondary goat anti-mouse Alexa 647 (1:500). Confocal microscopy was obtained using a Zeiss LSM 700 Inverted confocal laser scanning microscope. An excitation wavelength of 578 nm and an emission wavelength of 640 nm and below were used for Alexa568, whereas an excitation wavelength of 651 nm and an emission wavelength of 640 nm and above were used for Alexa647. FRET was assessed with AxioVision FRET software, using the mathematical approach - Youvan's technique. Youvan's technique (Fc) is the basis of all correction measurement techniques (out of 4 techniques) in AxioVision FRET. It refers to corrected FRET values when three FRET filter sets are used. The measured values are corrected for the background (bg) and for the crosstalk from the donor (don) and the acceptor (acc). Calculation of the intensity values for FRET follow the formula: Fc = (fretgv - bg) - cfdon (dongv - bg) - cfacc (accgv - bg), where gv is the fluorescence value in every pixel and cf is a constant which is calculated for each of the samples with only one secondary antibody.

Pulldown of subpellicular microtubules-bound proteins (proteomics). These experiments aimed to determine the levels of LdPKAC3 binding to the subpellicular microtubules of *L. donovani* wild type (WT) and *Δldpkar3*. Microtubules of WT and

Δldpkar3 promastigotes, before and 5 hours after exposure to differentiation signal, were DDM-enriched as described above. Subsequently, proteins associated with this fraction were separated on 9% SDS-PAGE and a slice containing proteins at the molecular mass range of 35-42kDa was excised and subsequently subjected to mass spectrometry.

The proteins in the gel were reduced with 3 mM DTT (60ºC for 30 min), modified with 10 mM iodoacetamide in 100 mM ammonium bicarbonate (in the dark, room temperature for 30 min) and digested in 10% acetonitrile and 10 mM ammonium bicarbonate with modified trypsin (Promega) at a 1:10 enzyme-to-substrate ratio, overnight at 37ºC. The resulted peptides were desalted using C18 tips (Homemade stage tips) dried and resuspended in 0.1% Formic acid**.**

The peptides were resolved by reverse-phase chromatography on 0.075 X 180-mm fused silica capillaries (J&W) packed with Reprosil reversed phase material (Dr Maisch GmbH, Germany). The peptides were eluted with linear 60 minutes gradient of 5 to 28%, 15 minutes gradient of 28 to 95% and 15 minutes at 95% acetonitrile with 0.1% formic acid in water at flow rates of 0.15 µl/min. Mass spectrometry was performed by Q Exactive plus mass spectrometer (Thermo) in a positive mode using repetitively full MS scan followed by collision induced dissociation (HCD) of the 10 most dominant ions selected from the first MS scan.

The mass spectrometry data was analyzed using Proteome Discoverer 1.4 software with Sequest (Thermo) algorithm against *L. donovani* and *L. infantum* proteomes from TriTryp database with mass tolerance of 20 ppm for the precursor masses and 0.05 Da for the fragment ions (TriTrypDB). Oxidation on Met, and Phosphorylation on Ser, Thr, Tyr were accepted as variable modifications and

Carbamidomethyl on Cys was accepted as static modifications. Minimal peptide length was set to six amino acids and a maximum of two miscleavages was allowed. Peptide- and protein-level false discovery rates (FDRs) were filtered to 1% using the target-decoy strategy. Semi-quantitation was done by calculating the peak area of each peptide based on its extracted ion currents (XICs) and the area of the protein that is the average of the three most intense peptides from each protein.

The mass spectrometry proteomics data have been deposited to the ProteomeXchange Consortium via the PRIDE [68] partner repository with the dataset identifier PXD025222.

Molecular modelling. LdPKAR3 homology models were built from each of the PDB templates 2QCS, 5JR7 and 4MX3 with Chimera Modeller [69,70]. The pairwise alignments used as input for threading PKAR3 and PKAC3 were extracted from multiple sequence alignments that included PKAR1 and PKAC1/C2, respectively, and were produced with Clustal Omega [71]. The R3/C3 complex was obtained by docking C3 into R3 using PDB template 2QCS as a guide, followed by energy minimization. Structure images were produced with UCSF Chimera [72].

Supplementary figure legends

Figure S1: Deleting *LdPKAR3* gene (A) and raising rabbit antibodies against LdPKAR3 protein. (B) PCR on genomic DNA extracted from promastigotes of WT (+/+) and a *Δldpkar3* (-/-). LdPKAR3 ORF (upper panel) is seen only on DNA extracted from WT cells, while the mutant contains both the resistance, hygromycin and neomycin (middle and bottom panels, respectively). (B) Proteins extracted from L. donovani WT (+/+; left lane), *Δldpkar3* (-/-; middle lane) and *Δldpkar3* ectopically expressing the full length LdPKAR3 (-/-/+; addback; right lane) were separated on 10% SDS-PAGE and subsequently subjected to Western Blot using the antibodies raised against LdPKAR3. Tubulin was used as loading control.

Figure S2: Deleting *LdPKAC3* from *L. donovani* genome. PCR on extracted genomic DNA from wild type (+/+) (**A**) or (**B**) *Δldpkac3* (-/-) cells. PKAC3 ORF is detected only in wild type cells, while *Δldpkac3* cells possess both resistance marker cassettes; hygromycin and neomycin.

Figure S3: A-B subpellicular microtubule enrichment using 0.5 % DDM; (**A**) The DDM-insoluble fraction is enriched with tubulin. Western blot of promastigote hole cell lysate (left lane) and 0.5% DDM insoluble fraction followed by Ponceau red staining. Anti β tubulin used as loading control. (**B**) DDM-insoluble subpellicular microtubules of axenic promastigotes (left panel) and amastigotes (right panel) were stained with anti β tubulin mouse antibodies (red). (**C**) Purity assessment of the DDM-insoluble fraction

from *L. donovani* promastigotes. Hole cell lysates (left lane) and DDM-insoluble fraction were stained with anti AAP24 (proline transporter, upper panels) and anti HSP30 (lower panels). (**D**) The rabbit anti LdPKAR3 activity in WT (upper panel) and Δ*ldpkar3* mutant (lower panel).

Figure S4: FRET control experiment. To determine the fluorescence level of each of the Alexa Fluor dyes that are coupled to the secondary antibodies used in the analysis described in Fig. 5C, (A) only LdPKAR3 was stained with Alexa Fluor 568 (in green) or (B) only ectopic LdPKAC3 (HA-tagged) was stained with Alexa 647 (in red). FRET analysis was carried out using Axio Vision program (STAR Methods).

Figure S5. Image streamer calibration with cell shape of *L. donovani* promastigotes and amastigotes. An Amnis® ImageStream®X Mk II image streamer was fed with either late log phase axenic promastigotes (A, upper panel) or axenic amastigotes (A, lower panel). For each life stage 10000 cells were tested, an image snapshot was taken (B) and subsequently an aspect ratio was calculated. The streamer divided these populations into three groups, elongated (marked in orange), round (red) and the intermediate shape named ovoid (pink). Note that round promatigotes are flagellated whereas round.

Bibliography

1. Maxfield, L., and Crane, J.S. (2020). Leishmaniasis. In: StatPearls [Internet]. Treasure Island (FL): StatPearls Publishing; 2021.
2. Zhang, W.W., Charest, H., and Matlashewski, G. (1995). The expression of biologically active human p53 in *Leishmania* cells: a novel eukaryotic system to produce recombinant proteins. Nucleic.Acids.Res. *23*, 4073–4080.
3. Alvar, J., Velez, I.D., Bern, C., Herrero, M., Desjeux, P., Cano, J., Jannin, J., den Boer, M., and Team, W.H.O.L.C. (2012). Leishmaniasis worldwide and global estimates of its incidence. PLoS One *7*, e35671.
4. Ruepp, B.U., Bohren, K.M., and Gabbay, K.H. (1997). Characterization of an element resembling an androgen response element (ARE) in the human aldose reductase promoter. In Advances in Experimental Medicine and Biology, pp. 515–519.
5. Chang, K.P., and Dwyer, D.M. (1976). Multiplication of a human parasite (*Leishmania donovani*) in phagolysosomes of hamster macrophages in vitro. Science (80-.). *193*, 678–680.
6. Herwaldt, B.L. (1999). Leishmaniasis. Lancet *354*, 1191–1199.
7. Bachmaier, S., Witztum, R., Tsigankov, P., Koren, R., Boshart, M., and Zilberstein, D. (2016). Protein kinase A signaling during bidirectional axenic differentiation in *Leishmania*. Int J Parasitol *46*, 75–82.
8. Zilberstein, D. (2008). Physiological and biochemical aspects of *Leishmania* develpment. In *Leishmania* after the genome: biology and control, P. J. Myler and N. Fasel, eds. (Horizon Scientific Press and Caiser Academic Press), pp. 107–122.
9. Barak, E., Amin-Spector, S., Gerliak, E., Goyard, S., Holland, N., and Zilberstein, D.

(2005). Differentiation of *Leishmania donovani* in host-free system: analysis of signal perception and response. Mol Biochem Parasitol *141*, 99–108.

10. Burchmore, R.J., and Barrett, M.P. (2001). Life in vacuoles--nutrient acquisition by *Leishmania* amastigotes. Int J Parasitol *31*, 1311–1320.

11. Saar, Y., Ransford, A., Waldman, E., Mazareb, S., Amin-Spector, S., Plumblee, J., Turco, S.J., and Zilberstein, D. (1998). Characterization of developmentally-regulated activities in axenic amastigotes of *Leishmania donovani*. Mol Biochem Parasitol *95*, 9–20.

12. Zilberstein, D., and Nitzan Koren, R. (2019). Host-Free Systems for Differentiation of Axenic *Leishmania*. In (Humana Press, New York, NY), pp. 1–8.

13. Courret, N., Frehel, C., Prina, E., Lang, T., and Antoine, J.C. (2001). Kinetics of the intracellular differentiation of *Leishmania amazonensis* and internalization of host MHC molecules by the intermediate parasite stages. Parasitology *122*, 263–279.

14. Tsigankov, P., Gherardini, P.F., Helmer-Citterich, M., Spaeth, G.F., Myler, P.J., and Zilberstein, D. (2014). Regulation dynamics of *Leishmania* differentiation: deconvoluting signals and identifying phosphorylation trends. Mol Cell Proteomics *13*, 1769–1786.

15. Taylor, S.S., Ilouz, R., Zhang, P., and Kornev, A.P. (2012). Assembly of allosteric macromolecular switches: lessons from PKA. Nat Rev Mol Cell Biol *13*, 646–658.

16. Wong, W., and Scott, J.D. (2004). AKAP signalling complexes: focal points in space and time. Nat Rev Mol Cell Biol *5*, 959–970.

17. Bubis, J., Martinez, J.C., Calabokis, M., Ferreira, J., Sanz-Rodriguez, C.E., Navas, V., Escalona, J.L., Guo, Y., and Taylor, S.S. (2018). The gene product of a *Trypanosoma equiperdum* ortholog of the cAMP-dependent protein kinase regulatory subunit is a monomeric protein that is not capable of binding cyclic nucleotides. Biochimie *146*, 166–

180.

18. Peng, M., Aye, T.T., Snel, B., van Breukelen, B., Scholten, A., and Heck, A.J. (2015). Spatial Organization in Protein Kinase A Signaling Emerged at the Base of Animal Evolution. J Proteome Res *14*, 2976–2987.

19. Bachmaier, S., Volpato Santos, Y., Kramer, S., Githure, G.B., Klöckner, T., Pepperl, J., Baums, C., Schenk, R., Schwede, F., Genieser, H.-G., et al. (2019). Nucleoside analogue activators of cyclic AMP-independent protein kinase A of *Trypanosoma*. Nat. Commun. *10*, 1421-1435.

20. Bachmaier, S., and Boshart, M. (2013). Kinetoplastid AGC kinases. In Protein phosphorylation in eukaryotic parasites: potential for chemotherapy, D. Doerig, C. S. Spaeth, M. Wiese, and P. M. Selzer, eds. (Wiley-Blackwell).

21. Tsigankov, P., Gherardini, P.F., Helmer-Citterich, M., Spath, G.F., and Zilberstein, D. (2013). Phosphoproteomic analysis of differentiating *Leishmania* parasites reveals a unique stage-specific phosphorylation motif. J Proteome Res *12*, 3405–3412.

22. Oberholzer, M., Langousis, G., Nguyen, H.T., Saada, E.A., Shimogawa, M.M., Jonsson, Z.O., Nguyen, S.M., Wohlschlegel, J.A., and Hill, K.L. (2011). Independent analysis of the flagellum surface and matrix proteomes provides insight into flagellum signaling in mammalian-infectious *Trypanosoma brucei*. Mol Cell Proteomics *10*, 1-14.

23. Fort, C., Bonnefoy, S., Kohl, L., and Bastin, P. (2016). Intraflagellar transport is required for the maintenance of the trypanosome flagellum composition but not its length. J. Cell Sci. *129*, 3026–41.

24. Chiasson, D., Giménez-Oya, V., Bircheneder, M., Bachmaier, S., Studtrucker, T., Ryan, J., Sollweck, K., Leonhardt, H., Boshart, M., Dietrich, P., et al. (2019). A unified multi-

kingdom Golden Gate cloning platform. Sci. Rep. *9*, 10131.

25. Rosenzweig, D., Smith, D., Opperdoes, F., Stern, S., Olafson, R.W., and Zilberstein, D. (2008). Retooling *Leishmania* metabolism: from sand fly gut to human macrophage. FASEB J *22*, 590–602.

26. Flegontov, P., Votýpka, J., Skalický, T., Logacheva, M.D., Penin, A.A., Tanifuji, G., Onodera, N.T., Kondrashov, A.S., Volf, P., Archibald, J.M., et al. (2013). *Paratrypanosoma* is a novel early-branching trypanosomatid. Curr. Biol. *23*, 1787–1793.

27. Gull, K. (1999). The cytoskeleton of trypanosomatid parasites. Annu Rev Microbiol *53*, 629–655.

28. Kohl, L., and Gull, K. (1998). Molecular architecture of the *Trypanosome* cytoskeleton. Mol Biochem Parasitol *93*, 1–9.

29. Dwyer, D.M. (1980). Isolation and partial characterization of surface membranes from *Leishmania donovani* promastigotes. J Protozool *27*, 176–182.

30. Dacheux, D., Landrein, N., Thonnus, M., Gilbert, G., Sahin, A., Wodrich, H., Robinson, D.R., and Bonhivers, M. (2012). A MAP6-related protein is present in protozoa and is involved in flagellum motility. PLoS One *7*, e31344.

31. Robinson, D., Beattie, P., Sherwin, T., and Gull, K. (1991). Microtubules, tubulin, and microtubule-associated proteins of trypanosomes. Methods Enzym. *196*, 285–299.

32. Sherwin, T., and Gull, K. (1989). The cell division cycle of *Trypanosoma brucei* brucei: timing of event markers and cytoskeletal modulations. Philos Trans R Soc L. B Biol Sci *323*, 573–588.

33. Inbar, E., Schlisselberg, D., Suter Grotemeyer, M., Rentsch, D., and Zilberstein, D. (2013). A versatile proline-alanine transporter in the unicellular pathogen *Leishmania*

donovani regulates amino acid homeostasis and osmotic stress responses. Biochem J *449*, 555–566.

34. Vicente-Manzanares, M., and Sanchez-Madrid, F. (2000). Cell polarization: a comparative cell biology and immunological view. Dev.Immunol. *7*, 51–65.

35. Ilouz, R., Lev-Ram, V., Bushong, E.A., Stiles, T.L., Friedmann-Morvinski, D., Douglas, C., Goldberg, G., Ellisman, M.H., and Taylor, S.S. (2017). Isoform-specific subcellular localization and function of protein kinase A identified by mosaic imaging of mouse brain. Elife *6*.

36. Faix, J., and Grosse, R. (2006). Staying in Shape with Formins. Dev. Cell *10*, 693–706.

37. Gordon, G.W., Berry, G., Liang, X.H., Levine, B., and Herman, B. (1998). Quantitative fluorescence resonance energy transfer measurements using fluorescence microscopy. Biophys. J. *74*, 2702-2713.

38. Ciruela, F., Vilardaga, J.P., and Fernández-Dueñas, V. (2010). Lighting up multiprotein complexes: Lessons from GPCR oligomerization. Trends Biotechnol. *28* , 4070415.

39. Bruystens, J.G., Wu, J., Fortezzo, A., Del Rio, J., Nielsen, C., Blumenthal, D.K., Rock, R., Stefan, E., and Taylor, S.S. (2016). Structure of a PKA RIalpha Recurrent Acrodysostosis Mutant Explains Defective cAMP-Dependent Activation. J Mol Biol *428*, 4890–4904.

40. Bruystens, J.G., Wu, J., Fortezzo, A., Kornev, A.P., Blumenthal, D.K., and Taylor, S.S. (2014). PKA RIalpha homodimer structure reveals an intermolecular interface with implications for cooperative cAMP binding and Carney complex disease. Structure *22*, 59–69.

41. Kim, C., Cheng, C.Y., Saldanha, S.A., and Taylor, S.S. (2007). PKA-I holoenzyme structure reveals a mechanism for cAMP-dependent activation. Cell *130*, 1032–1043.

42. Barros, E.P., Malmstrom, R.D., Nourbakhsh, K., Del Rio, J.C., Kornev, A.P., Taylor, S.S., and Amaro, R.E. (2017). Electrostatic Interactions as Mediators in the Allosteric Activation of Protein Kinase A RIalpha. Biochemistry *56*, 1536–1545.

43. Lee, Y., Wang, Q., Shuryak, I., Brenner, D.J., and Turner, H.C. (2019). Development of a high-throughput γ-H2AX assay based on imaging flow cytometry. Radiat. Oncol. *14*, 150.

44. Oliveira, M., Joao Rodrigues, M., Pereira, C., Neto, R., Junior, P.A.S., Neng, N.D.R., Nogueira, J.M.F., Varela, J., Barreira, L., and Custodio, L. (2018). First report of the in vitro antileishmanial properties of extremophile plants from the Algarve Coast. Nat Prod Res *32*, 600–604.

45. Rodrigues, M.A. (2018). Automation of the in vitro micronucleus assay using the Imagestream® imaging flow cytometer. Cytom. Part A *93*, 706–726.

46. Zilberstein, D., and Shapira, M. (1994). The role of pH and temperature in the development of *Leishmania* parasites. Annu Rev Microbiol *48*, 449–470.

47. Antoine, J.C., Prina, E., Jouanna, C., and Bongrand, P. (1990). Parasitophorous vacuoles of *Leishmania amazonensis* - infected macrophages maintain an acidic pH. Infect.Immun. *58*, 779–787.

48. Zilberstein, D. (2021). Lysosome sensing is a key mechanism in *Leishmania* intracellular development. Front. Microbiol. *Accepted*.

49. Bertiaux, E., Morga, B., Blisnick, T., Rotureau, B., and Bastin, P. (2018). A Grow-and-Lock Model for the Control of Flagellum Length in *Trypanosomes*. Curr. Biol. *28*, 3802-3814.e3.

50. Kohl, L., and Bastin, P. (2005). The flagellum of trypanosomes. Int. Rev. Cytol. *244*, 227–285.

51. Halliday, C., Billington, K., Wang, Z., Dean, S., Sunter, J.D., and Wheeler, R.J. (2018). Cellular landmarks of *Trypanosoma brucei* and *Leishmania mexicana*. Mol Biochem Parasitol. *230*, 24-36.

52. Sunter, J.D., Moreira-Leite, F., and Gull, K. (2018). Dependency relationships between IFT-dependent flagellum elongation and cell morphogenesis in *Leishmania*. Open Biol. *8*.

53. Svitkina, T. (2018). The actin cytoskeleton and actin-based motility. Cold Spring Harb. Perspect. Biol. *10*.

54. Riquelme, M., Aguirre, J., Bartnicki-García, S., Braus, G.H., Feldbrügge, M., Fleig, U., Hansberg, W., Herrera-Estrella, A., Kämper, J., Kück, U., et al. (2018). Fungal Morphogenesis, from the Polarized Growth of Hyphae to Complex Reproduction and Infection Structures. Microbiol. Mol. Biol. Rev. *82*.

55. Sündermann, F., Fernandez, M.P., and Morgan, R.O. (2016). An evolutionary roadmap to the microtubule-associated protein MAP Tau. BMC Genomics *17* 264-280.

56. Wallar, B.J., and Alberts, A.S. (2003). The formins: active scaffolds that remodel the cytoskeleton. Trends Cell Biol *13*, 435–446.

57. Bartolini, F., and Gundersen, G.G. (2010). Formins and microtubules. Biochim Biophys Acta *1803*, 164–173.

58. Haushalter, K.J., Casteel, D.E., Raffeiner, A., Stefan, E., Patel, H.H., and Taylor, S.S. (2018). Phosphorylation of protein kinase A (PKA) regulatory subunit RIalpha by protein kinase G (PKG) primes PKA for catalytic activity in cells. J Biol Chem *293*, 4411–4421.

59. Stamatakis, A. (2014). RAxML version 8: A tool for phylogenetic analysis and post-analysis of large phylogenies. Bioinformatics *30*, 1312–1313.

60. Blum, M., Chang, H.Y., Chuguransky, S., Grego, T., Kandasaamy, S., Mitchell, A., Nuka,

G., Paysan-Lafosse, T., Qureshi, M., Raj, S., et al. (2021). The InterPro protein families and domains database: 20 years on. Nucleic Acids Res. *49*, D344–D354.

61. Zimmermann, L., Stephens, A., Nam, S.Z., Rau, D., Kübler, J., Lozajic, M., Gabler, F., Söding, J., Lupas, A.N., and Alva, V. (2018). A Completely Reimplemented MPI Bioinformatics Toolkit with a New HHpred Server at its Core. J. Mol. Biol. *430*, 2237–2243.

62. Gabler, F., Nam, S.Z., Till, S., Mirdita, M., Steinegger, M., Söding, J., Lupas, A.N., and Alva, V. (2020). Protein Sequence Analysis Using the MPI Bioinformatics Toolkit. Curr. Protoc. Bioinforma. *72*.

63. Vassella, E., Reuner, b, Yutzy, b, and Boshart, M. (1997). Differentiation of African Trypanosones is controlled by density sensing mechanism which signals cell cycle arrest via the cAMP pathway. J. Cell Sci. *110*, 2661–2671.

64. Darlyuk, I., Goldman, A., Roberts, S.C., Ullman, B., Rentsch, D., and Zilberstein, D. (2009). Arginine homeostasis and transport in the human pathogen *Leishmania donovani*. J Biol Chem *284*, 19800–19807.

65. Biebinger, S., Elizabeth Wirtz, L., Lorenz, P., and Clayton, C. (1997). Vectors for inducible expression of toxic gene products in bloodstream and procyclic *Trypanosoma brucei*. Mol. Biochem. Parasitol. *85*, 99–112.

66. Alibu, V.P., Storm, L., Haile, S., Clayton, C., and Horn, D. (2005). A doubly inducible system for RNA interference and rapid RNAi plasmid construction in *Trypanosoma brucei*. Mol. Biochem. Parasitol. *139*, 75–82.

67. Bastin, P., Bagherzadeh, A., Matthews, K.R., and Gull, K. (1996). A novel epitope tag system to study protein targeting and organelle biogenesis in *Trypanosoma brucei*. Mol.

Biochem. Parasitol. *77*, 235–239.

68. Perez-Riverol, Y., Csordas, A., Bai, J., Bernal-Llinares, M., Hewapathirana, S., Kundu, D.J., Inuganti, A., Griss, J., Mayer, G., Eisenacher, M., et al. (2019). The PRIDE database and related tools and resources in 2019: Improving support for quantification data. Nucleic Acids Res. *47*, D442–D450.

69. Meng, E.C., Pettersen, E.F., Couch, G.S., Huang, C.C., and Ferrin, T.E. (2006). Tools for integrated sequence-structure analysis with UCSF Chimera. BMC Bioinformatics *7*, 339.

70. Webb, B., and Sali, A. (2014). Comparative Protein Structure Modeling Using MODELLER. Curr Protoc Bioinforma. *47*, 5 6 1-32.

71. Sievers, F., and Higgins, D.G. (2018). Clustal Omega for making accurate alignments of many protein sequences. Protein Sci *27*, 135–145.

72. Pettersen, E.F., Goddard, T.D., Huang, C.C., Couch, G.S., Greenblatt, D.M., Meng, E.C., and Ferrin, T.E. (2004). UCSF Chimera--a visualization system for exploratory research and analysis. J Comput Chem *25*, 1605–1612.

Figure 1

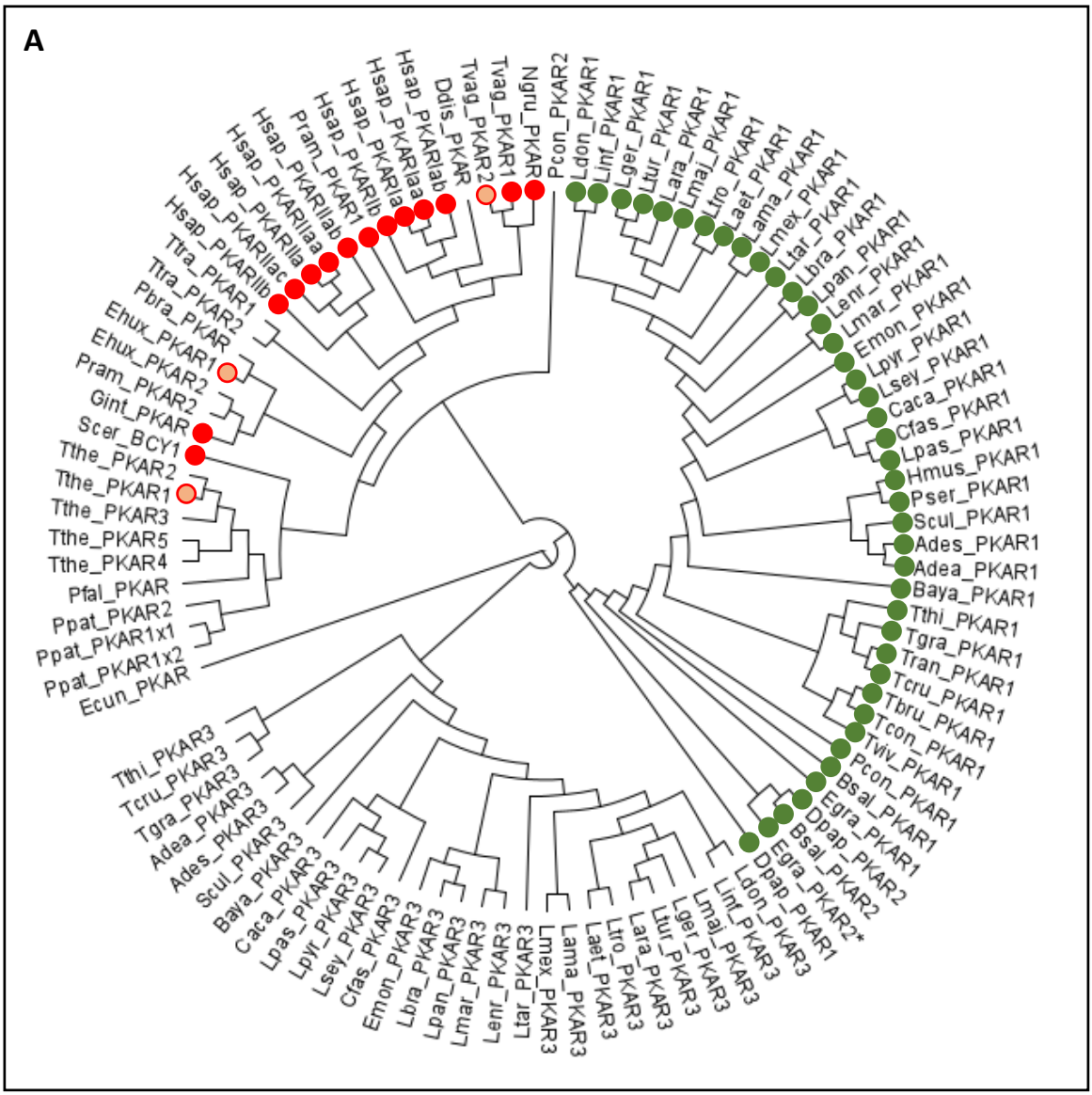
A
Hsap_PKARIa
Hsap_PKARIaa
Hsap_PKARIab
Hsap_PKARIb
Hsap_PKARIIa
Hsap_PKARIIaa
Hsap_PKARIIab
Hsap_PKARIIac
Hsap_PKARIIb
Pram_PKAR1
Ddis_PKAR
Tvag_PKAR2
Tvag_PKAR1
Ngru_PKAR
Pcon_PKAR2
Ldon_PKAR1
Lint_PKAR1
Lger_PKAR1
Ltur_PKAR1
Lara_PKAR1
Lmaj_PKAR1
Ltro_PKAR1
Laet_PKAR1
Lama_PKAR1
Lmex_PKAR1
Ltar_PKAR1
Lbra_PKAR1
Lpan_PKAR1
Lenr_PKAR1
Lmar_PKAR1
Emon_PKAR1
Lpyr_PKAR1
Lsey_PKAR1
Caca_PKAR1
Cfas_PKAR1
Lpas_PKAR1
Hmus_PKAR1
Pser_PKAR1
Scul_PKAR1
Ades_PKAR1
Adea_PKAR1
Baya_PKAR1
Tthi_PKAR1
Tgra_PKAR1
Tran_PKAR1
Tcru_PKAR1
Tbru_PKAR1
Tcon_PKAR1
Tviv_PKAR1
Pcon_PKAR1
Bsal_PKAR1
Egra_PKAR1
Dpap_PKAR1
Bsal_PKAR2
Egra_PKAR2*
Dpap_PKAR2
Ldon_PKAR3
Lint_PKAR3
Lmaj_PKAR3
Lger_PKAR3
Ltur_PKAR3
Lara_PKAR3
Ltro_PKAR3
Laet_PKAR3
Lama_PKAR3
Lmex_PKAR3
Ltar_PKAR3
Lenr_PKAR3
Lmar_PKAR3
Lpan_PKAR3
Lbra_PKAR3
Emon_PKAR3
Cfas_PKAR3
Lsey_PKAR3
Lpyr_PKAR3
Lpas_PKAR3
Caca_PKAR3
Baya_PKAR3
Scul_PKAR3
Ades_PKAR3
Adea_PKAR3
Tgra_PKAR3
Tcru_PKAR3
Tthi_PKAR3
Ecun_PKAR
Ppat_PKAR1x2
Ppat_PKAR1x1
Ppat_PKAR2
Pfal_PKAR
Tthe_PKAR4
Tthe_PKAR5
Tthe_PKAR3
Tthe_PKAR1
Tthe_PKAR2
Scer_BCY1
Gint_PKAR
Pram_PKAR2
Ehux_PKAR1
Ehux_PKAR
Pbra_PKAR
Ttra_PKAR2
Ttra_PKAR1
B
Hsap_PKARIa
Ddis_PKAR
Scer_BCY1
Ppat_PKAR2
Ldon_PKAR1
Ldon_PKAR3

Figure 2

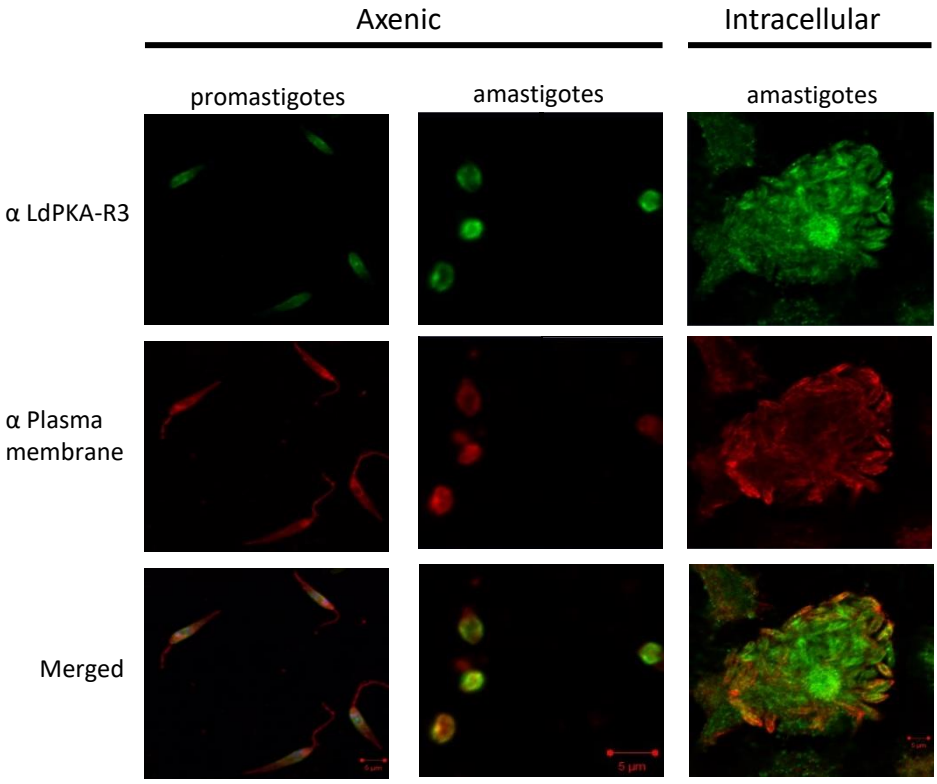
Axenic
Intracellular
promastigotes
amastigotes
amastigotes
α LdPKA-R3
α Plasma membrane
Merged
5 µm

Figure 3

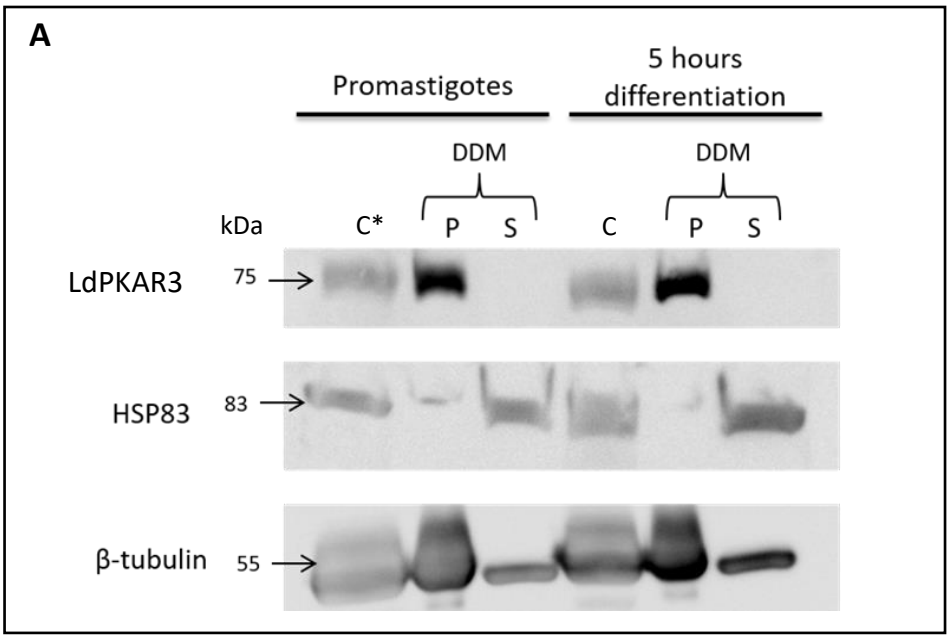
A
Promastigotes
5 hours differentiation
DDM
DDM
kDa
C*
P
S
C
P
S
LdPKAR3
75
HSP83
83
β-tubulin
55

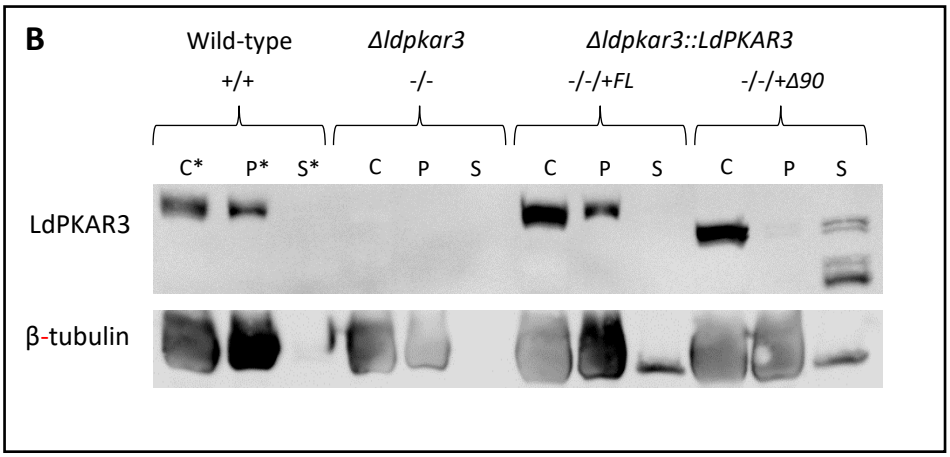
B
Wild-type
+/+
Δldpkar3
-/-
Δldpkar3::LdPKAR3
-/-/+FL
-/-/+Δ90
C*
P*
S*
C
P
S
C
P
S
C
P
S
LdPKAR3
β-tubulin

Figure 4

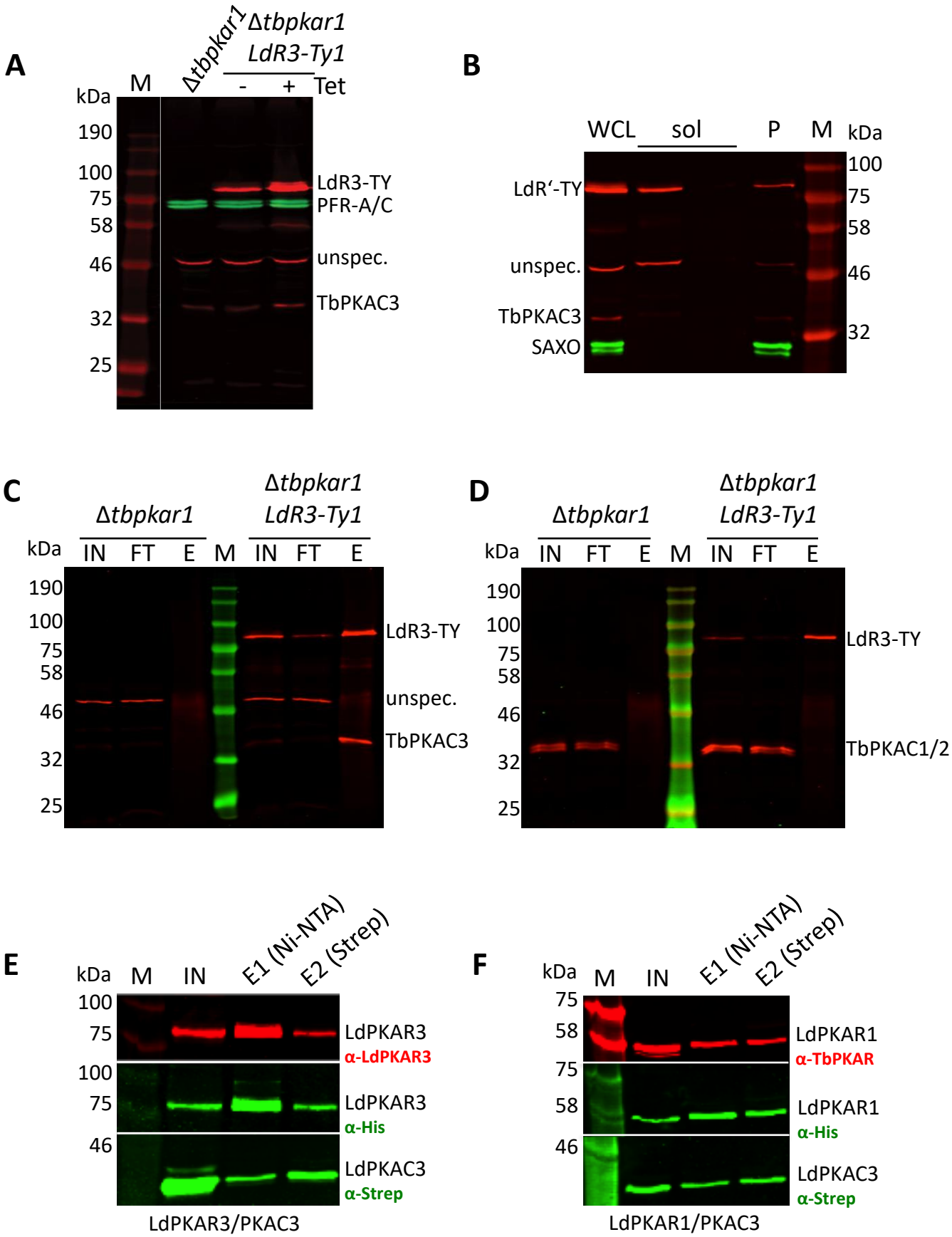
A
kDa
M
Δtbpkar1
Δtbpkar1
LdR3-Ty1
-
+
Tet
190
100
75
58
46
32
25
LdR3-TY
PFR-A/C
unspec.
TbPKAC3
B
WCL
sol
P
M
kDa
LdR'-TY
unspec.
TbPKAC3
SAXO
100
75
58
46
32
C
Δtbpkar1
Δtbpkar1
LdR3-Ty1
kDa
IN
FT
E
M
IN
FT
E
190
100
75
58
46
32
25
LdR3-TY
unspec.
TbPKAC3
D
Δtbpkar1
Δtbpkar1
LdR3-Ty1
kDa
IN
FT
E
M
IN
FT
E
190
100
75
58
46
32
25
LdR3-TY
TbPKAC1/2
E
kDa
M
IN
E1 (Ni-NTA)
E2 (Strep)
100
75
100
75
46
LdPKAR3
α-LdPKAR3
LdPKAR3
α-His
LdPKAC3
α-Strep
LdPKAR3/PKAC3
F
kDa
M
IN
E1 (Ni-NTA)
E2 (Strep)
75
58
75
58
46
LdPKAR1
α-TbPKAR
LdPKAR1
α-His
LdPKAC3
α-Strep
LdPKAR1/PKAC3

Figure 5

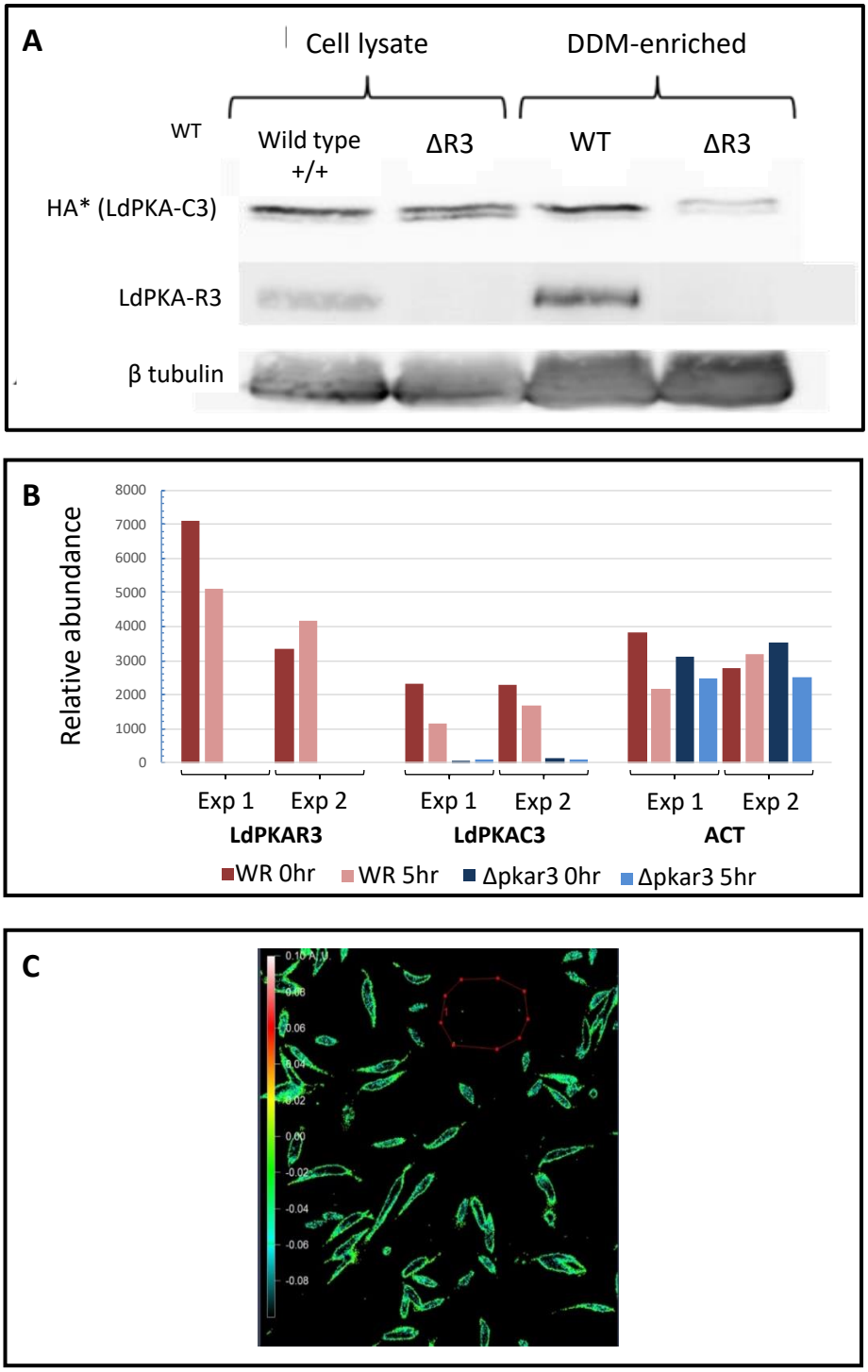
A
Cell lysate
DDM-enriched
WT
Wild type +/+
ΔR3
WT
ΔR3
HA* (LdPKA-C3)
LdPKA-R3
β tubulin
B
Relative abundance
8000
7000
6000
5000
4000
3000
2000
1000
0
Exp 1
Exp 2
LdPKAR3
Exp 1
Exp 2
LdPKAC3
Exp 1
Exp 2
ACT
WR 0hr
WR 5hr
Δpkar3 0hr
Δpkar3 5hr
C
0.10
0.08
0.06
0.04
0.02
0.00
-0.02
-0.04
-0.06
-0.08

Figure 6

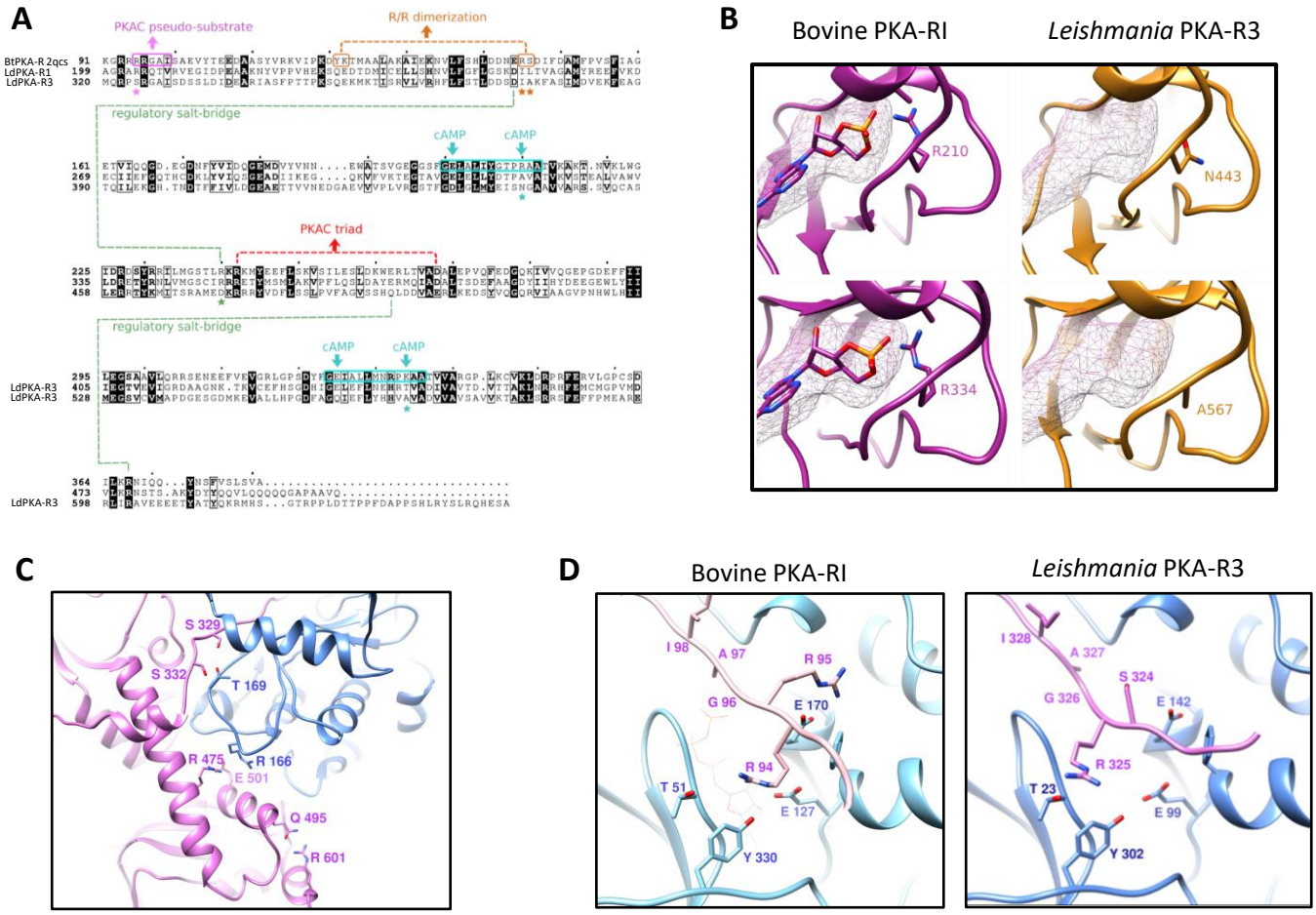
A
PKAC pseudo-substrate
R/R dimerization
BtPKA-R 2qcs
LdPKA-R1
LdPKA-R3
regulatory salt-bridge
cAMP
cAMP
PKAC triad
regulatory salt-bridge
cAMP
cAMP
LdPKA-R3
LdPKA-R3
LdPKA-R3
B
Bovine PKA-RI
Leishmania PKA-R3
R210
N443
R334
A567
C
S 329
S 332
T 169
R 475
R 166
E 501
Q 495
R 601
D
Bovine PKA-RI
Leishmania PKA-R3
I 98
A 97
R 95
G 96
E 170
R 94
T 51
E 127
Y 330
I 328
A 327
S 324
G 326
E 142
R 325
T 23
E 99
Y 302

Figure 7

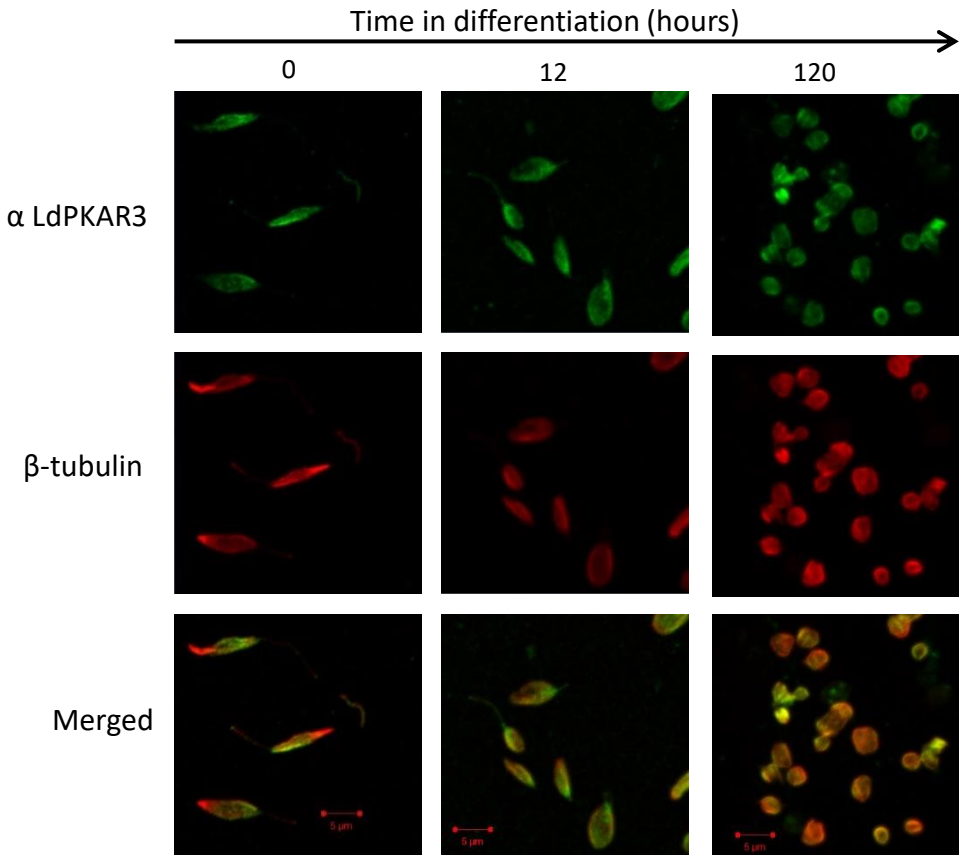
Time in differentiation (hours)
0
12
120
α LdPKAR3
β-tubulin
Merged

Figure 8

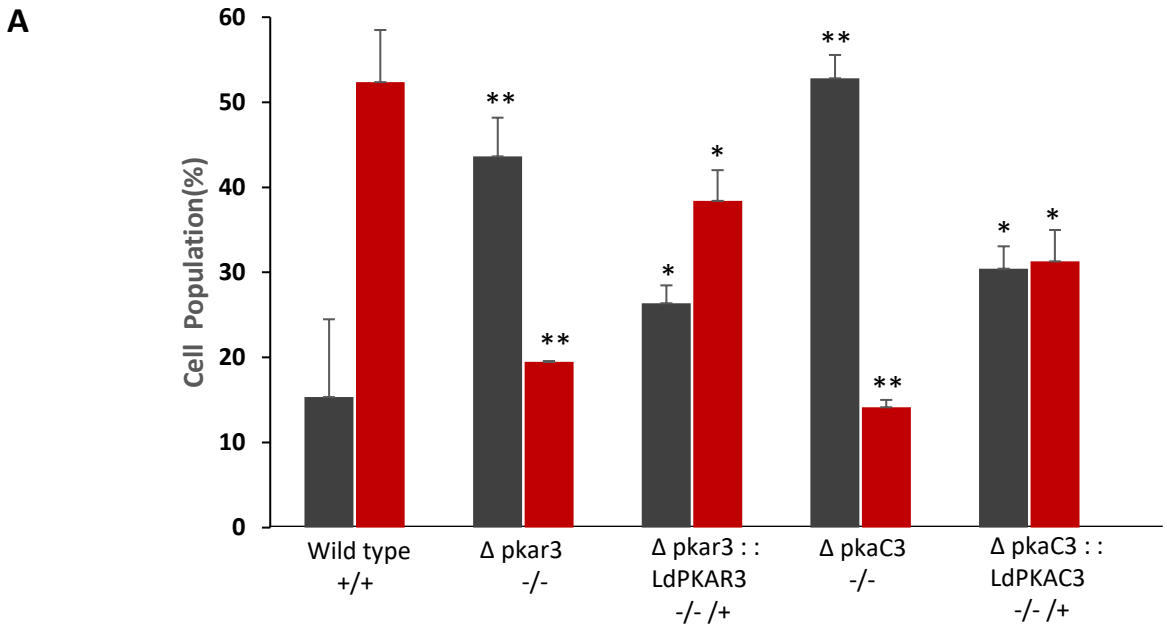
A
Cell Population(%)
60
50
40
30
20
10
0
**
**
*
*
**
**
*
*
Wild type
+/+
Δ pkar3
-/-
Δ pkar3 : :
LdPKAR3
-/- /+
Δ pkaC3
-/-
Δ pkaC3 : :
LdPKAC3
-/- /+

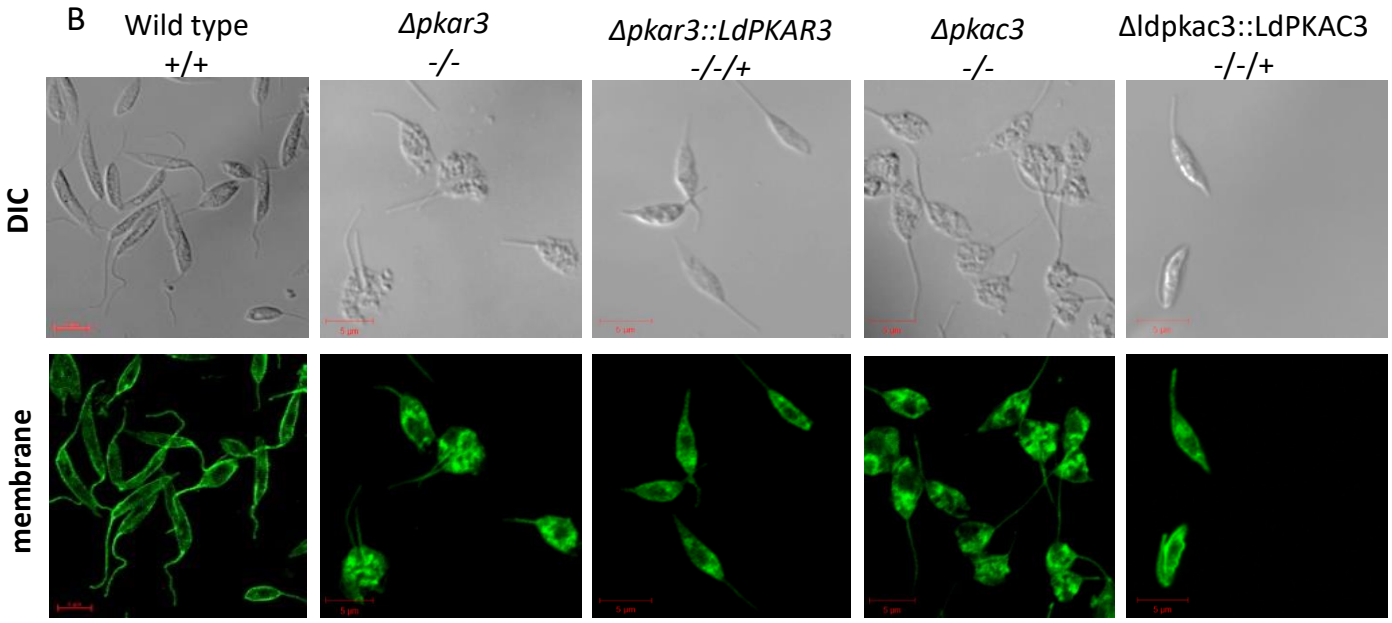
B
Wild type
+/+
Δpkar3
-/-
Δpkar3::LdPKAR3
-/-/+
Δpkac3
-/-
Δldpkac3::LdPKAC3
-/-/+
DIC
Anti-
membrane